

Entanglement in Gauge/Gravity Duality

by

Sunok Josephine Suh

Submitted to the Department of Physics
in partial fulfillment of the requirements for the degree of

Doctor of Philosophy

at the

MASSACHUSETTS INSTITUTE OF TECHNOLOGY

June 2015

[September 2015]

© Massachusetts Institute of Technology 2015. All rights reserved.

Author . ¹
Signature redacted

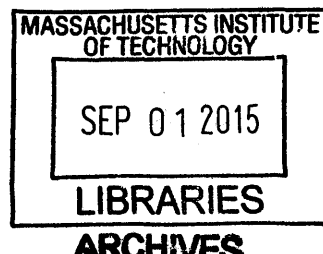
.....
Department of Physics
April 30, 2015

Certified by ¹
Signature redacted

.....
Hong Liu
Professor of Physics
Thesis Supervisor

Accepted by ¹
Signature redacted

.....
Nergis Mavalvala
Associate Department Head for Education



Entanglement in Gauge/Gravity Duality

by

Sunok Josephine Suh

Submitted to the Department of Physics
on April 30, 2015, in partial fulfillment of the
requirements for the degree of
Doctor of Philosophy

Abstract

In this thesis, we present studies that elucidate the relationship between entanglement in strongly coupled gauge theories and the geometry of their gravity duals. In the first, we find that in a certain class of time-dependent states which have a gravity dual in which a black hole forms, the entanglement entropy of large regions grows linearly in time, following the growth of certain time-like slices in the interior of the black hole. In the second, we find a unified prescription in the gravity dual for calculating the action of the entanglement Hamiltonian associated to an arbitrary spatial region in a given holographic state. In particular, we find that the linearized perturbation of the metric caused by the entanglement Hamiltonian propagates from the bulk entangling surface.

Thesis Supervisor: Hong Liu

Title: Professor of Physics

Contents

1	Introduction	13
1.1	Introduction	13
1.2	Holographic entanglement entropy conjecture	14
1.3	Real-space entanglement renormalization	14
2	Growth of Entanglement and the Interior of Black Holes	17
2.1	States dual to AdS-Vaidya geometries	17
2.2	Extremal surface solutions	26
2.3	Linear growth	36
3	The Gravity Duals of Entanglement Hamiltonians	49
3.1	Entanglement Hamiltonians	49
3.2	Modular response	54
3.3	Propagation of metric response	65
3.4	Further directions	67
4	Conclusions	71

List of Figures

2-1 Vaidya geometry: One patches pure AdS with a black hole along an in-falling collapsing null shell located at $v = 0$. We take the width of the shell to be zero which corresponds to the $\delta t = 0$ limit of the boundary quench process. The spatial directions along the boundary are suppressed in the figure. 18

2-2 Cartoon of the curve $(z_t(R, t), v_t(R, t))$ for (a) continuous and (b) discontinuous saturation. Cartoons of various extremal surfaces whose tip are labelled above are shown in Fig. 2-3. (a): For continuous saturation the whole curve has a one-to-one correspondence to (R, t) , and saturation happens at point C continuously. (b): Discontinuous saturation happens via a jump of the extremal surface from one with tip at C' to one with tip at C . Along the dashed portion of the curve, different points can correspond to the same (R, t) 33

2-3 Cartoons of extremal surfaces with tip at various points labelled in Fig. 2-2. Spatial directions are suppressed. (a): At $t = 0_+$, the extremal surface starts intersecting the null shell, with z_c very small. (b) When $t \gtrsim z_h$, the extremal surface starts intersecting the null shell behind the horizon. (c) The extremal surface close to continuous saturation for which $z_t - z_c$ is small. 33

2-4	Parametric curves $(z_t(R, t), z_c(R, t))$ at fixed R and varying t for Schwarzschild $h(z)$ in $d = 3$. Different curves correspond to $R = 2, 3, \dots, 10$. In both plots, we choose units so that the horizon is at $z_h = 1$. (a): For a strip. Note the saturation is discontinuous with z_c lying behind the horizon at the saturation point where each curve stops. (b): For a sphere. The saturation is continuous and z_c lies outside the horizon at the saturation point (in the plot it is too close to the horizon to be discerned).	35
2-5	In the limit of a large z_t and a finite $z_c \approx z_c^*$, the evolution in the black hole region is essentially solely in the time direction, with two sides of the strip evolving independently.	43
2-6	A cartoon of an extremal surface for Σ with some arbitrary shape, in the large size limit and t in the linear regime. Upon entering the black hole region, the extremal surface has essentially attained its boundary shape Σ . The evolution in the black hole region is essentially solely in the time direction and is the same as that for a strip.	44
2-7	Cartoon: For a sphere, in the linear regime the extremal surface follows the critical extremal surface for a while but exits near the first plateau. The dashed curve is the critical extremal surface.	47
3-1	Cartoon of the diffeomorphism-invariant support of the modular response $\partial_\alpha h \approx (g_\alpha - g)/\alpha$, as computed using the HRT prescription. The entanglement wedge of R , whose intersection with the AdS boundary is $\mathcal{C}(R)$, is delineated in pink. Left: for configurations (ρ, R) with special symmetry, the response is causal from ∂R . Right: for generic (ρ, R) the response is causal from the entire extremal surface associated with R . To avoid clutter here we have only drawn the upper half of time evolution.	53
3-2	Riemannian sheets for Euclidean path integrals corresponding to the operator $\rho_R^k \otimes I$, left, and ρ_R , right.	57

- 3-3 Depiction of a geodesic in Poincaré AdS which computes the expectation value of an equal-time two-point function $\langle \mathcal{O}(x)\mathcal{O}(y) \rangle$, with x and y in Rindler regions $\mathcal{C}(\bar{R})$ and $\mathcal{C}(R)$, where R is the half-space $x_1 \geq 0$. (Note we have $d = 2$ in the figure for ease of drawing, but all considerations here are in $d \geq 3$ for which there are local gravitational excitations in the bulk.) The light-cone and boundary light-cone from ∂R are shown in solid beige and transparent purple, respectively. The solid purple line is the extremal surface E . All contributions to $\partial_\alpha \langle \mathcal{O}(x)\mathcal{O}(y) \rangle$ come from the intersection of the geodesic with the boundary light-cone from ∂R 63
- 3-4 Tests of the scaling of I in (3.32) in $d = 3$ and at $\varepsilon = 10^{-3}$. The fixed parameters in each plot are as follows - left: $y^1 = -x^1 = 11$, $\Delta x^2 = 0$, center: $t = 1$, $x^1 = -3/2$, $\Delta x^2 = 0$, right: $t = 1$, $y^1 = -x^1 = 3/2$ 65
- 3-5 A component of the Weyl response on an interior point of E for an R which is a slab in $d = 3$ with finite extent $-1 \leq x^1 \leq 1$ and extending infinitely in remaining boundary spatial coordinate x^2 . Left: The point on E at which we measure the Weyl response. We show a $t = t_R$, $x^2 = \text{const.}$ cross section of the bulk space-time g which is Poincaré AdS. Right: The component $\partial_\alpha C_{z_2 t_2}$ on the point specified as a function of the light-cone cutoff ε . It diverges as $\varepsilon \rightarrow 0$ 69

List of Tables

Chapter 1

Introduction

1.1 Introduction

Since the discovery of an anti-de Sitter space/conformal field theory duality in [52], and subsequent elaboration of a dictionary relating boundary conditions of bulk fields to sources and expectation values for corresponding operators in the boundary theory [28, 72], we have known that gravitational degrees of freedom can emerge from those of an ordinary quantum field theory on a fixed background in one less dimension.

In examples of AdS/CFT [52, 2], in the limit of strong 't Hooft coupling and large N in the boundary gauge theory, the dual gravitational theory is decoupled from strings and has a small Newton's constant G_N . Thus we expect the Hilbert space of fluctuations of a quantum field theory weakly coupled to gravity in an asymptotically anti-de Sitter background, to emerge from the strong dynamics of certain large- N gauge theories which can be taken to live on the time-like boundary of said anti-de Sitter space.

This emergence of gravity from gauge theory is expected to be quite general and has been dubbed gauge/gravity duality [36]. A pressing and open question in the context of such a duality is how local degrees of freedom far from the boundary in the gravitational theory are mapped to boundary degrees of freedom.

1.2 Holographic entanglement entropy conjecture

A significant hint regarding the above question came in the form of the Ryu-Takayanagi conjecture [63] - that the entanglement entropy

$$S = -\text{Tr}(\rho \log \rho) \tag{1.1}$$

of the reduced density matrix ρ of a spatial region, in a time-independent state of a large- N field theory that is sharply peaked around a classical bulk configuration is to lowest order in $1/N$, is given by the area, in units of $1/G_N$, of the bulk surface with minimal area ending on the boundary of the spatial region [63]. In addition to considerable evidence, a derivation has been provided in [45], which only relies on the widely established facet of gauge/gravity duality in which the saddle point of the gravitational partition function, equal to the boundary path integral, is given by a bulk configuration satisfying equations of motion.

A covariant generalization of the Ryu-Takayanagi conjecture has been given [38], in which minimal surfaces are replaced by extremal surfaces, and the quantum field theory state can be time-dependent. This generalization has been shown to be consistent with strong subadditivity [4, 15, 71] and boundary causality [32], but has not yet been given a proof.

Taken together, the above conjectures point to a tangible relationship between quantum entanglement in the boundary quantum field theory and the emergence of a bulk spacetime including an extra dimension [69]. For example, linearized Einstein's equations about the anti-de Sitter vacuum have been derived [22] using the Ryu-Takayanagi and Hubeny-Takayanagi-Rangamani conjectures, and the first law of entanglement entropy [10].

1.3 Real-space entanglement renormalization

Another facet of the Ryu-Takayanagi conjecture is that it has made manifest the relationship between a certain class of tensor-network representations for many-body

ground states that are conformal in the IR, dubbed the multi-scale entanglement renormalization ansatz (MERA) [70], and the geometry of anti-de Sitter space [21, 66, 67]. MERA tensor networks, in which real-space entanglement is renormalized away in incremental steps, and an unentangled state is produced as an output, seem to reproduce the geometry of anti-de Sitter space on scales larger than the AdS radius.

More recently, a continuous version of MERA has been proposed [30] which is suited to describing the real-space entanglement renormalization of *continuum* field theories. It has been suggested that the geometry of gravity duals can be directly derived in the cMERA formalism [57], although a seeming obstacle to investigating this so far has been that there are no analytic examples of cMERA for interacting theories. Here we will not pursue this topic further.

In this thesis, we present studies that further elucidate the relationship between entanglement in strongly coupled gauge theories with gravity duals, and the geometry of their gravity duals.

In the first chapter, we find using the Hubeny-Rangamani-Takayanagi conjecture, that in a certain class of time-dependent states which have a gravity dual in which a black hole forms, the entanglement entropy of large regions grows linearly in time, following the growth of certain time-like slices in the interior of the black hole. This provides a direct example in which the entanglement properties of a quantum field theory state are able to encode information behind even global horizons.

In the second chapter, we find prescriptions in the gravity dual for calculating the action of an entanglement or modular Hamiltonian associated to a spatial region, or minus the logarithm of the corresponding reduced density matrix, where the spatial region can be arbitrary and the quantum field theory is only restricted by the requirement that it has a gravity dual. In particular, we find to linear order in the action of the entanglement Hamiltonian, that the perturbation of the metric in the dual geometry is an integral of the graviton-graviton propagator over the Ryu-Takayanagi surface.

Chapter 2

Growth of Entanglement and the Interior of Black Holes

2.1 States dual to AdS-Vaidya geometries

In this chapter we consider the evolution of entanglement entropy after a sharp quench of a strongly coupled *gapless* system with a gravity dual. More explicitly, at $t = 0$ in the boundary system we turn on a spatially uniform density of external sources for an interval δt , creating a spatially homogeneous and isotropic excited state with nonzero energy density, which subsequently equilibrates. The precise manner (e.g. what kind of sources are turned on and how) through which the excited state is generated and its microscopic details will not concern us. We are interested in the macroscopic behavior of the system at large distances and in extracting “universal” behavior in the evolution of these observables that are insensitive to the specific nature of final equilibrium states.

On the gravity side such a quench process is described by a thin shell of matter starting from the boundary and collapsing to form a black hole, which can in turn be described by a Vaidya metric, see Fig. 2-1. The matter fields making up the shell and their configuration are determined by the sourcing process in the boundary theory and are again not important for our purposes. See e.g. [7, 46, 26, 5, 73, 47, 74] for more explicit discussions. In the classical gravity regime we are working with, which

translates to the large N and strongly coupled limit of the boundary theory, all of our observables are only sensitive to the metric of the collapsing geometry.

We give a detailed description of our setup and review the vacuum and equilibrium properties of the class of systems under consideration.

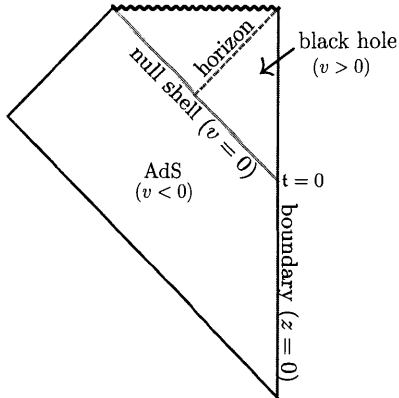


Figure 2-1: Vaidya geometry: One patches pure AdS with a black hole along an in-falling collapsing null shell located at $v = 0$. We take the width of the shell to be zero which corresponds to the $\delta t = 0$ limit of the boundary quench process. The spatial directions along the boundary are suppressed in the figure.

2.1.1 Vaidya metric

We consider a metric of the form

$$ds^2 = \frac{L^2}{z^2} (-f(v, z)dv^2 - 2dv dz + d\vec{x}^2) . \quad (2.1)$$

In the limit the sourcing interval δt goes to zero, the width of the collapsing shell goes to zero and $f(v, z)$ can be expressed in terms of a step function

$$f(v, z) = 1 - \theta(v)g(z) . \quad (2.2)$$

For $v < 0$, the metric is given by that of pure AdS,

$$ds^2 = \frac{L^2}{z^2} (-dt^2 + dz^2 + d\vec{x}^2) \quad (2.3)$$

where

$$v = t - z , \quad t = v + z . \quad (2.4)$$

For $v > 0$, (2.1) is given by that of a black hole in Eddington-Finkelstein coordinates,

$$ds^2 = \frac{L^2}{z^2} \left(-h(z)dv^2 - 2dvdz + d\vec{x}^2 \right) , \quad (2.5)$$

which in terms of the usual Schwarzschild time t can be written as

$$ds^2 = \frac{L^2}{z^2} \left(-h(z)dt^2 + \frac{1}{h(z)}dz^2 + d\vec{x}^2 \right) \quad (2.6)$$

with

$$h(z) \equiv 1 - g(z) , \quad v = t - \sigma(z) , \quad \sigma(z) = \int_0^z \frac{dz'}{h(z')} . \quad (2.7)$$

The functions $h(z)$ in the black hole metric (2.5)–(2.6) may be interpreted as “parameterizing” different types of equilibration processes with different final equilibrium states. We assume that (2.1) with some $g(z)$ can always be achieved by choosing an appropriate configuration of matter fields. In following discussions we will not need the explicit form of $h(z)$, and only that it gives rise to a black hole metric. We will work with a general boundary spacetime dimension d .

More explicitly, we assume $h(z)$ has a simple zero at the horizon $z = z_h > 0$, and that for $z < z_h$, it is positive and monotonically decreasing as a function of z as required by the IR/UV connection. As we approach the boundary, i.e. as $z \rightarrow 0$, $h(z)$ approaches zero with the leading behavior

$$h(z) = 1 - Mz^d + \dots \quad (2.8)$$

where M is some constant. From (2.8), one obtains that the energy density of the equilibrium state is

$$\mathcal{E} = \frac{L^{d-1}}{8\pi G_N} \frac{d-1}{2} M , \quad (2.9)$$

while its temperature and entropy density are given by

$$T = \frac{|h'(z_h)|}{4\pi}, \quad s_{\text{eq}} = \frac{L^{d-1}}{z_h^{d-1}} \frac{1}{4G_N}. \quad (2.10)$$

Representative examples of (2.5) include the AdS Schwarzschild black hole with

$$h(z) = 1 - \frac{z^d}{z_h^d} \quad (2.11)$$

which describes a neutral final equilibrium state, and the AdS Reissner-Nordstrom (RN) black hole with

$$h(z) = 1 - Mz^d + Q^2 z^{2d-2}, \quad (2.12)$$

which describes a final equilibrium state with a nonzero chemical potential for some conserved charge.

A characteristic scale of the black hole geometry (2.5)–(2.6) is the horizon size¹ z_h which from (2.10) can be expressed in terms of the entropy density s_{eq} as

$$z_h = \left(\frac{L^{d-1}}{4G_N} \frac{1}{s_{\text{eq}}} \right)^{\frac{1}{d-1}}. \quad (2.13)$$

Were we considering a gas of quasiparticles, the prefactor $\frac{L^{d-1}}{4G_N}$ in (2.13) could be interpreted as the number of internal degrees of freedom of a quasiparticle, and z_h would then be the average distance between quasiparticles, or mean free path. Here of course we are considering strongly coupled systems which do *not* have a quasiparticle description. Nevertheless, z_h provides a characteristic scale of the equilibrium state. For example, as we will see below it controls the correlation length of equal-time correlation functions and Wilson loops in equilibrium.

For the collapsing process described by (2.1) we can also identify z_h as a “local equilibrium scale” ℓ_{eq} , which can be defined as the time scale when the system has ceased production of thermodynamic entropy, or in other words, has achieved local

¹Note that while the horizon location is a coordinate dependent quantity, in the particular radial coordinate used in (2.5)–(2.6) z_h corresponds to a meaningful boundary scale as for example indicated by (2.13).

equilibrium at distance scales of order the “mean free path” of the equilibrium state. We will discuss further support for this identification at the end of Sec. 2.2.3.

We note that in the AdS Schwarzschild case (2.11), the temperature T is the only scale and controls both the local equilibrium scale z_h and energy density \mathcal{E} (given by (2.9)),

$$T = \frac{d}{4\pi z_h}, \quad M = \frac{1}{z_h^d} = \left(\frac{4\pi T}{d}\right)^d, \quad (2.14)$$

but that in a system with more than one scale as in the Reissner-Nordstrom case, z_h and \mathcal{E} (or M) do not depend only on T . In the Reissner-Norstrom case, it is convenient to introduce a quantity

$$u \equiv \frac{4\pi z_h T}{d} \quad (2.15)$$

which decreases monotonically from its Schwarzschild value of unity to 0, as the chemical potential is increased from zero to infinity at fixed T . Thus with a large chemical potential (compared to temperature), the local equilibrium scale $\ell_{\text{eq}} \sim z_h$ can be much smaller than the thermal wave length $1/T$. In this regime, the system is controlled by finite density physics which gives rise to the scale z_h . For recent related discussions, see [19].

Finally, we note that the metric (2.1) is not of the most general form describing a spatially homogenous and isotropic equilibration process. If the equilibrium state has a nontrivial expectation value for (or sourced by) some scalar operators, the metric has the form

$$ds^2 = \frac{L^2}{z^2} (-f(v, z)dv^2 - 2q(v, z)dvdz + d\vec{x}^2) \quad (2.16)$$

with $f(v, z) = 1 - \theta(v)g(z)$ and $q(v, z) = 1 - \theta(v)m(z)$. The black hole part of the spacetime now has a metric of the form

$$ds^2 = \frac{L^2}{z^2} (-h(z)dv^2 - 2k(z)dvdz + d\vec{x}^2) \quad (2.17)$$

with $h(z) \equiv 1 - g(z)$ and $k(z) \equiv 1 - m(z)$, and can also be written as

$$ds^2 = \frac{L^2}{z^2} \left(-h(z)dt^2 + \frac{dz^2}{l(z)} + d\vec{x}^2 \right), \quad k^2(z) = \frac{h(z)}{l(z)}. \quad (2.18)$$

We will restrict our discussion mostly to (2.1), but it is straightforward to generalize our results to (2.16) as will be done in various places below.

2.1.2 Vacuum properties

Before the quench, our system is in the vacuum state of a strongly coupled CFT with a gravity dual. Consider an extremal surface Γ_Σ (with boundary Σ) in pure AdS, whose area gives the vacuum value of the corresponding physical observable. When Σ is a sphere,²

$$\begin{aligned} \mathcal{A}_{\text{sphere}} &= \text{local divergences} \\ &+ L^n \omega_{n-1} \begin{cases} (-1)^{\frac{n}{2}} b_n & n \text{ even} \\ (-1)^{\frac{n-1}{2}} b_n \log R & n \text{ odd} \end{cases} \end{aligned} \quad (2.19)$$

where ω_{n-1} is the area of unit $(n-1)$ -dimensional sphere and

$$b_n = \frac{(n-2)!!}{(n-1)!!}. \quad (2.20)$$

When Σ is a strip,

$$\begin{aligned} \mathcal{A}_{\text{strip}} &= \text{local divergences} + \begin{cases} 2L \log R & n = 1 \\ -\frac{L^n (a_n)^n}{n-1} \frac{A_{\text{strip}}}{R^{n-1}} & n > 1 \end{cases}, \\ a_n &\equiv \frac{\sqrt{\pi} \Gamma(\frac{1}{2} + \frac{1}{2n})}{\Gamma(\frac{1}{2n})} \end{aligned} \quad (2.21)$$

where A_{strip} is the area of the strip Σ with both sides included. The local divergences in (2.19) and (2.21) can be interpreted as coming from short-range correlations near

²The following expressions for Σ a sphere or strip have appeared in many places in the literature. For the case of entanglement entropy with $n = d - 1$, they were first obtained in [63].

Σ and its leading contributions are proportional to A_Σ .

The number of degrees of freedom in a CFT can be characterized by a central charge s_d , defined in all dimensions in terms of the universal part of the entanglement entropy of a spherical region in the vacuum [56],

$$S_{\text{sphere}}^{(\text{vac})} = \text{local divergences} + \begin{cases} (-1)^{\frac{d-1}{2}} s_d & d \text{ odd} \\ (-1)^{\frac{d-2}{2}} s_d \log R & d \text{ even} \end{cases}, \quad (2.22)$$

where from (2.19),

$$s_d = \frac{L^{d-1}}{4G_N} \omega_{d-2} b_{d-1} = \frac{\pi^{\frac{d}{2}} L^{d-1}}{\Gamma(\frac{d}{2}) 4G_N} \times \begin{cases} 1 & d \text{ odd} \\ \frac{2}{\pi} & d \text{ even} \end{cases}. \quad (2.23)$$

Note that for $d = 2$ the above central charge is related to the standard central charge c as

$$s_2 = \frac{c}{3}. \quad (2.24)$$

From the standard AdS/CFT dictionary, $s_d \propto N^2$ where N is the rank of the gauge group(s) of the boundary theory. If we put such a holographic CFT on a lattice, s_d is heuristically the number of degrees of freedom on a single lattice site.

From (2.19)–(2.21), a Wilson loop of circular and rectangular shape respectively have the vacuum behavior

$$W_\Sigma \sim \begin{cases} e^{-\#\sqrt{\lambda}} & \text{circle} \\ e^{-\#\sqrt{\lambda} \frac{\ell}{R}} & \text{rectangle} \end{cases}, \quad \sqrt{\lambda} = \frac{L^2}{\alpha'} \quad (2.25)$$

where ℓ denote the length of the long side of a rectangular Wilson loop. Similarly one finds that the two-point correlation function of an operator with large dimension $\Delta \approx mL \gg 1$ is given by

$$G(2R) \sim \frac{1}{R^{2\Delta}}. \quad (2.26)$$

2.1.3 Equilibrium properties

After the quench, our system eventually evolves to a final equilibrium state dual to a black hole in the bulk. Here we briefly review properties of an extremal surface Γ_Σ (with boundary Σ) in the black hole geometry (2.6), whose area gives the equilibrium value of the corresponding physical observable.

To leading order in large size limit, one can show that for Σ of any shape [48]

$$\mathcal{A}_\Sigma^{(\text{eq})} = \frac{L^n V_\Sigma}{z_h^n} \equiv \mathbf{a}_{\text{eq}} V_\Sigma, \quad \mathbf{a}_{\text{eq}} = \frac{L^n}{z_h^n}, \quad (2.27)$$

where V_Σ denotes the volume of the boundary region bounded by surface Σ , and \mathbf{a}_{eq} can be interpreted as an equilibrium “density.” This result has a simple geometric interpretation in the bulk – in the large size limit, most of the extremal surface simply runs along the horizon. In particular, for entanglement entropy,

$$S_\Sigma^{(\text{eq})} = \frac{L^{d-1}}{4G_N} \frac{V_\Sigma}{z_h^{d-1}} = s_{\text{eq}} V_\Sigma \quad (2.28)$$

where we have used the entropy density s_{eq} from (2.10). For a Wilson loop we have

$$W_{\text{eq}} \sim e^{-\#\sqrt{\lambda} \frac{V_\Sigma}{z_h^2}} \quad (2.29)$$

where V_Σ is now the area of the region enclosed by the loop. The two-point correlation function of an operator with dimension $\Delta \approx mL \gg 1$ is given by

$$G_{\text{eq}}(2R) \sim e^{-\Delta \frac{2R}{z_h}}. \quad (2.30)$$

2.1.4 Further comments

It should be kept in mind that while the final equilibrium state has a temperature and coarse grained thermal entropy density, the Vaidya geometry describes the evolution of a pure state. As a consistency check, one can show that for such a process the entanglement entropy for a region A is the same as that of its complement [1, 3, 68].

Thus the equilibrium entanglement entropy (2.28), despite having a thermal form, reflects genuine long-range quantum entanglement. The reason (2.28) has exactly the form of a thermal entropy is as follows. We are considering a finite region in a system of infinite size. Thus the number of degrees of freedom outside the region is always infinitely larger than that inside. As a result in a typical excited pure state the reduced density matrix for the finite region appears thermal [58].

Before the quench, our system is in a vacuum state of a CFT and thus already has long range correlations, whereas the initial state of [14] only has short-range correlations. However, this difference is likely not important for the questions we are interested in, which concern the build-up of the finite density of entanglement entropy in (2.28). The long-range entanglement in the vacuum, quantified by the universal part in (2.22), is measure zero compared to (2.28). Heuristically, for odd d , the long-range entanglement entropy in the vacuum, being a R -independent constant, amounts to that of a few sites inside the region that are fully entangled with the outside, while in equilibrium, almost all points inside the region become entangled. For even d , there is a logarithmic enhancement of the long-range entanglement in the vacuum, but it is still measure zero compared to the final entanglement in the large region limit.

From the perspective of entanglement entropy, the equilibration process triggered by the quench builds up long-range entanglement, as can be seen by comparing (2.28) and (2.22), whereas from the perspective of correlation functions and Wilson loops in which \mathcal{A} appears in the exponential with a minus sign, the same process corresponds to the destruction of correlations (compare (2.29)–(2.30) with (2.25)–(2.26)). More specifically, long range correlations in the latter observables which were present in the vacuum are replaced by short-range correlations with correlation length controlled by z_h . However, there is no contradiction, as the process of building up entanglement also involves redistribution of those in the vacuum – pre-existing correlations between local operators and over the Wilson loop get diluted by the redistribution process.

2.2 Extremal surface solutions

Here we describe equations of motion for Γ_Σ and its general characteristics when Σ is a strip or a sphere. In such cases Γ_Σ can be described by two functions, $z(\rho), v(\rho)$ for a sphere, or $z(x_1), v(x_1)$ for a strip. For both shapes the functions satisfy the following boundary conditions at the boundary as well as regularity conditions at the tip of the surface,

$$z(R) = 0, \quad v(R) = \mathfrak{t}, \quad z'(0) = v'(0) = 0. \quad (2.31)$$

For a strip we will write x_1 simply as x . It is convenient to introduce the location (z_t, v_t) of the tip of Γ_Σ ,

$$z(0) = z_t, \quad v(0) = v_t. \quad (2.32)$$

The sphere and strip being highly symmetric, specifying (z_t, v_t) completely fixes Γ_Σ . The relations between (R, \mathfrak{t}) and (z_t, v_t) are in general rather complicated and require solving the full equations for $z(\rho), v(\rho)$ or $z(x), v(x)$. Also, it is possible that a given (R, \mathfrak{t}) corresponds to multiple (z_t, v_t) 's, i.e. multiple extremal surfaces have the same boundary data. Then as mentioned earlier we will choose the extremal surface with smallest area.

For Σ a sphere or strip we will simply denote $\mathcal{A}_\Sigma(\mathfrak{t})$ as $\mathcal{A}(R, \mathfrak{t})$.

2.2.1 Strip

The area of an n -dimensional surface in (2.1) ending on a strip Σ can be written as

$$\mathcal{A} = \frac{1}{2} \tilde{K} \int_{-R}^R dx \frac{\sqrt{Q}}{z^n}, \quad Q \equiv 1 - 2v'z' - f(z, v)v'^2 \quad (2.33)$$

where

$$\tilde{K} = L^n A_{\text{strip}}, \quad (2.34)$$

with A_{strip} being the area of Σ (both sides of Σ are included which gives the $\frac{1}{2}$ factor in (2.33)). $z(x), v(x)$ then satisfy the equations of motion

$$z^n \sqrt{Q} \partial_x \left(\frac{z' + f v'}{z^n \sqrt{Q}} \right) = \frac{1}{2} \frac{\partial f}{\partial v} v'^2, \quad (2.35)$$

$$z^n \sqrt{Q} \partial_x \left(\frac{v'}{z^n \sqrt{Q}} \right) = n \frac{Q}{z} + \frac{1}{2} \frac{\partial f}{\partial z} v'^2. \quad (2.36)$$

Since the integrand of \mathcal{A} does not depend explicitly on x , there is a first integral

$$z^n \sqrt{Q} = J = \text{const}. \quad (2.37)$$

Furthermore, when $\partial_v f = 0$, equation (2.35) can be integrated to give another first integral,

$$z' + f v' = E = \text{const}. \quad (2.38)$$

We are mainly interested in Γ_Σ which go through both AdS and black hole regions. With reflection symmetry about $x = 0$, we only need to consider the $x > 0$ half of such a Γ_Σ . We now discuss equations in each region separately:

1. AdS region: From (2.31) and (2.38) we have

$$E = z' + v' = 0 \quad (2.39)$$

and from (2.37)

$$z' = -\frac{1}{z^n} \sqrt{J^2 - z^{2n}}, \quad J = z_t^n, \quad (2.40)$$

which give

$$x(z) = \int_z^{z_t} \frac{dy y^n}{\sqrt{z_t^{2n} - y^{2n}}}, \quad v(z) = v_t + z_t - z. \quad (2.41)$$

2. Matching conditions at the shell: Denoting the values of z and x at the intersection of Γ_Σ and the null shell $v = 0$ as z_c and x_c , respectively, we have

$$z_c = z_t + v_t \quad (2.42)$$

and derivatives on the AdS side of the null shell are

$$z'_- = -v'_- = -\frac{1}{z_c^n} \sqrt{z_t^{2n} - z_c^{2n}} . \quad (2.43)$$

To find derivatives on the other side, we integrate the equations of motion (2.35)–(2.36) across the null shell to find the matching conditions

$$\begin{aligned} v'_+ &= v'_- , & Q_+ &= Q_- , \\ z'_+ &= z'_- + \frac{1}{2}g(z_c)v' = \left(1 - \frac{1}{2}g(z_c)\right) z'_- . \end{aligned} \quad (2.44)$$

Note we have used the subscript $-$ ($+$) to refer to quantities on the AdS (black hole) side of the null shell.

3. Black hole region: From matching conditions (2.44), J is the same as in the AdS region, i.e. given by (2.40), while E is given by

$$E = \frac{1}{2}g(z_c)z'_- < 0 \quad (2.45)$$

implying t is no longer constant. From (2.38),

$$v' = \frac{E - z'}{h} \quad (2.46)$$

which can be substituted into (2.37) to obtain

$$z'^2 = h(z) \left(\frac{z_t^{2n}}{z^{2n}} - 1 \right) + E^2 \equiv H(z) . \quad (2.47)$$

Substituting (2.47) back in (2.46) we also have

$$\frac{dv}{dz} = -\frac{1}{h} \left(\frac{E}{\sqrt{H}} + 1 \right) . \quad (2.48)$$

Collecting equations in the two regions we find from (2.40) and (2.47)

$$R = \int_{z_c}^{z_t} \frac{dz}{\sqrt{\frac{z_t^{2n}}{z^{2n}} - 1}} + \int_0^{z_c} \frac{dz}{\sqrt{H(z)}}, \quad (2.49)$$

where we have assumed that $z(x)$ monotonically decreases as x increases (recall we let $x > 0$). As we will see later $z(x)$ can be non-monotonic in which case the above equation should be suitably modified. Similar caveats should be kept in mind for other equations below. From integrating (2.48),

$$\mathfrak{t} = \int_0^{z_c} \frac{dz}{h(z)} \left(\frac{E}{\sqrt{H(z)}} + 1 \right). \quad (2.50)$$

Note that at $z = z_h$, $h(z)^{-1}$ has a pole but the integrand in (2.50) remains finite as the second factor vanishes at $z = z_h$, due to $H(z_h) = E^2$ and $E < 0$. Finally, from (2.40) and (2.47) we have that the area of Γ_Σ is given by

$$\mathcal{A} = \mathcal{A}_{AdS} + \mathcal{A}_{BH} \quad (2.51)$$

where

$$\frac{1}{\tilde{K}} \mathcal{A}_{AdS} = z_t^{1-n} \int_{\frac{z_c}{z_t}}^1 dy \frac{1}{y^n \sqrt{1 - y^{2n}}} \quad (2.52)$$

and

$$\frac{1}{\tilde{K}} \mathcal{A}_{BH} = z_t^n \int_0^{z_c} dz \frac{1}{z^{2n} \sqrt{H(z)}}. \quad (2.53)$$

For a given R and \mathfrak{t} , we can use (2.49) and (2.50) to solve for $z_t(R, \mathfrak{t})$, $z_c(R, \mathfrak{t})$ after which (2.51) can be expressed in terms of R and \mathfrak{t} .

2.2.2 Sphere

The area of an n -dimensional surface in (2.1) ending on a sphere Σ can be written as

$$\mathcal{A} = K \int_0^R d\rho \frac{\rho^{n-1}}{z^n} \sqrt{Q}, \quad Q = 1 - 2v'z' - f(z, v)v'^2 \quad (2.54)$$

where

$$K = L^n \frac{A_{\text{sphere}}}{R^{n-1}} . \quad (2.55)$$

It follows that $z(\rho), v(\rho)$ satisfy the equations of motion

$$\frac{z^n \sqrt{Q}}{\rho^{n-1}} \partial_\rho \left[\frac{\rho^{n-1}}{z^n} \frac{1}{\sqrt{Q}} v' \right] = \frac{nQ}{z} + \frac{1}{2} \frac{\partial f}{\partial z} v'^2 , \quad (2.56)$$

$$\frac{z^n \sqrt{Q}}{\rho^{n-1}} \partial_\rho \left[\frac{\rho^{n-1}}{z^n} \frac{1}{\sqrt{Q}} (z' + f v') \right] = \frac{1}{2} \frac{\partial f}{\partial v} v'^2 , \quad (2.57)$$

and boundary conditions (2.31). When $\partial_v f = 0$, equation (2.57) can be integrated to give

$$\frac{\rho^{n-1}}{z^n} \frac{1}{\sqrt{Q}} (z' + f v') = E = \text{const} \quad (2.58)$$

which can also be expressed as

$$\frac{\rho^{n-1}}{z^n} \frac{f}{\sqrt{Q}} \frac{dt}{d\rho} = E \quad (2.59)$$

where t is the Schwarzschild time.

Again, we are interested in Γ_Σ which go through both AdS and black hole regions:

1. AdS region: Given (2.31), we again have $E = 0$, which implies that the solution in the AdS region is the same as that in pure AdS, i.e. is given by [62]

$$z(\rho) = \sqrt{z_t^2 - \rho^2} , \quad v(\rho) = z_t + v_t - z(\rho) . \quad (2.60)$$

2. Matching conditions at the shell: Denoting values of z and ρ at the intersection of Γ_Σ and the null shell $v = 0$ as z_c and ρ_c , respectively, we have

$$z_c = z_t + v_t , \quad \rho_c = \sqrt{z_t^2 - z_c^2} \quad (2.61)$$

and derivatives on the AdS side of the null shell are

$$z'_- = -v'_- = -\frac{\rho_c}{z_c} . \quad (2.62)$$

To find the corresponding derivatives on the other side, we integrate (2.56) and (2.57) across the shell, which again leads to the matching conditions (2.44) but with z'_- , v'_- now as in (2.62).

3. Black hole region: The matching implies

$$E = -\frac{1}{2} \left(\frac{\rho_c}{z_c} \right)^n \frac{g(z_c)}{z_t} < 0 \quad (2.63)$$

and t is no longer constant. Solving for v' and Q in terms of z' using (2.58), we obtain

$$v' = \frac{1}{h(z)} \left(-z' + \frac{EB\sqrt{1 + \frac{z'^2}{h}}}{\sqrt{1 + \frac{E^2 B^2}{h}}} \right), \quad B \equiv \frac{z^n}{\rho^{n-1}} \quad (2.64)$$

which, when substituted in (2.56), gives the equation for z

$$\begin{aligned} (h + E^2 B^2) z'' + (h + z'^2) \left(\frac{n-1}{\rho} z' + \frac{nh}{z} \right) \\ + (E^2 B^2 - z'^2) \frac{\partial_z h}{2} = 0. \end{aligned} \quad (2.65)$$

From integrating (2.64), the boundary time is

$$\begin{aligned} t &= \int_{\rho_c}^R \frac{d\rho}{h} \left(-z' + \frac{EB\sqrt{1 + \frac{z'^2}{h}}}{\sqrt{1 + \frac{E^2 B^2}{h}}} \right) \\ &= \int_{\rho_c}^R \frac{d\rho}{h + E^2 B^2} \frac{E^2 B^2 - z'^2}{EB\sqrt{\frac{h+z'^2}{h+E^2 B^2} + z'}} \end{aligned} \quad (2.66)$$

where the second expression is manifestly well-defined at the horizon, and the integral is evaluated on shell, with $z(\rho)$ satisfying equation (2.65) and boundary conditions (2.44) at $\rho = \rho_c$ and $z(R) = 0$. Finally, from (2.60) and (2.64), the area of Γ_Σ can be written as

$$\mathcal{A} = \mathcal{A}_{AdS} + \mathcal{A}_{BH} \quad (2.67)$$

where

$$\frac{1}{K} \mathcal{A}_{AdS} = \int_0^{\rho_c} d\rho \frac{\rho^{n-1}}{z^n} \sqrt{1+z'^2} = \int_0^{\frac{\rho_c}{z_t}} dx \frac{x^{n-1}}{(1-x^2)^{\frac{n+1}{2}}} \quad (2.68)$$

and

$$\frac{1}{K} \mathcal{A}_{BH} = \int_{\rho_c}^R d\rho \frac{\rho^{n-1}}{z^n} \frac{\sqrt{1+\frac{z'^2}{h}}}{\sqrt{1+\frac{E^2 B^2}{h}}} . \quad (2.69)$$

Note the story here is significantly more complicated than for a strip. One needs to first solve the differential equation (2.65) with initial condition given by the last equation of (2.44). Imposing the boundary condition $z(R) = 0$ gives a relation between ρ_c and z_c . One then needs to evaluate (2.66) to find $z_c(R, t)$, $\rho_c(R, t)$ and finally use (2.67) to obtain $\mathcal{A}(R, t)$.

2.2.3 Time evolution

We now describe geometric features of Γ_Σ during its time evolution, using as examples the case of Σ being a sphere or a strip. For the two shapes the equations of motion (given in Sec. 2.2) can be readily solved numerically. We are interested in long-distance behavior, i.e. we take

$$R \gg z_h . \quad (2.70)$$

At fixed R , as t is varied, the tip (2.32) of Γ_Σ traces out a curve $(z_t(R, t), v_t(R, t))$ in the Penrose diagram. This provides a nice way to visualize the evolution of Γ_Σ with t . See Fig. 2-2.

Instead of (z_t, v_t) it is sometimes convenient to use (z_t, z_c) or (z_t, ρ_c) to specify Γ_Σ , where z_c and ρ_c are the values of z and ρ at which the Γ_Σ intersects the null shell. For both sphere and strip $z_c = z_t + v_t$. For a sphere ρ_c is given by (2.61), while for a strip x_c can be obtained by setting $z = z_c$ in (2.41).

We now elaborate on various stages of the time evolution of Γ_Σ , and strategies for obtaining $\mathcal{A}(R, t)$ in each of them.

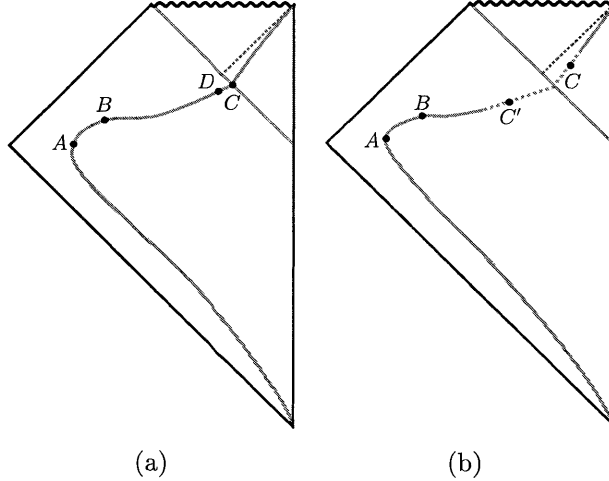


Figure 2-2: Cartoon of the curve $(z_t(R, t), v_t(R, t))$ for (a) continuous and (b) discontinuous saturation. Cartoons of various extremal surfaces whose tip is labelled above are shown in Fig. 2-3. (a): For continuous saturation the whole curve has a one-to-one correspondence to (R, t) , and saturation happens at point C continuously. (b): Discontinuous saturation happens via a jump of the extremal surface from one with tip at C' to one with tip at C . Along the dashed portion of the curve, different points can correspond to the same (R, t) .

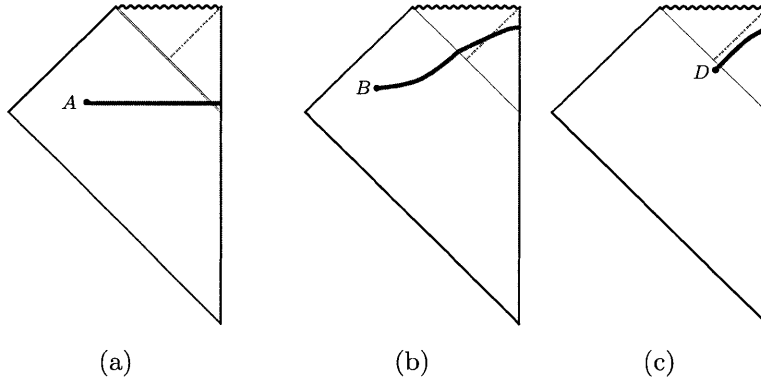


Figure 2-3: Cartoons of extremal surfaces with tip at various points labelled in Fig. 2-2. Spatial directions are suppressed. (a): At $t = 0_+$, the extremal surface starts intersecting the null shell, with z_c very small. (b) When $t \gtrsim z_h$, the extremal surface starts intersecting the null shell behind the horizon. (c) The extremal surface close to continuous saturation for which $z_t - z_c$ is small.

For $t < 0$, Γ_Σ lies entirely in AdS, and

$$z_t(R, t < 0) = \begin{cases} R & \text{sphere} \\ \frac{R}{a_n} & \text{strip} \end{cases}, \quad v_t = t - z_t \quad (2.71)$$

where a_n was introduced in (2.21). $\mathcal{A}(R, t)$ is independent of t and is given by its vacuum value. In Fig. 2-2 this corresponds to the part of curve below point A . Note that as $R \rightarrow \infty$, $z_t \rightarrow \infty$.

At $t = 0_+$, or point A , Γ_Σ starts intersecting the null shell (see Fig. 2-3(a)). For $t \ll z_h$, the point of intersection is close to the boundary, i.e. $z_c \ll z_h$. This defines the pre-local-equilibrium stage mentioned in the Introduction. In this regime, one can extract $\mathcal{A}_\Sigma(t)$ by expanding both t and \mathcal{A} in small z_c .

When t becomes of order z_h , at some point Γ_Σ starts intersecting the shell behind the horizon, i.e. $z_c > z_h$. An example is point B in Fig. 2-2, whose corresponding Γ_Σ is shown in Fig. 2-3(b).

There exists a sharp time t_s after which Γ_Σ lies entirely in the black hole region. Γ_Σ then reduces to that in a static black hole geometry. It lies on a constant Schwarzschild time $t = t$ outside the horizon and is time independent. That is, for $t > t_s$

$$z_t(R, t) = z_b(R) < z_h, \quad v_t = t - \sigma(z_t) \quad (2.72)$$

where z_b denotes the location of the tip of Γ_Σ in the static black hole geometry, and in the second equation we have used (2.7). This corresponds to the part of the curve above point C in Fig. 2-2. For $t > t_s$, $\mathcal{A}(R, t)$ is time independent and given by its equilibrium value.

The saturation at the equilibrium value at t_s can proceed as a continuous or discontinuous transition, as illustrated in Fig. 2-2. For a continuous transition, depicted on the left, the entire curve (z_t, v_t) as a function of t has one-to-one correspondence with (R, t) and saturation happens at point C , with t_s given by

$$v_t(t_s) = 0, \quad t_s(R) = \sigma(z_b(R)) = \int_0^{z_b} \frac{dz}{h(z)}. \quad (2.73)$$

In contrast, for a discontinuous saturation, depicted on the right plot of Fig. 2-2, in the dashed portion of the curve, there are multiple (z_t, v_t) associated with a given (R, t) . As a result, the minimal area condition requires that the extremal surface jump from point C' to C at some t_s . In this case there does not exist a general

formula for t_s . For a discontinuous saturation, $\mathcal{A}_\Sigma(t)$ is continuous at t_s , but its first time derivative becomes discontinuous.

In the case of a continuous saturation, for which the first time derivative of $\mathcal{A}_\Sigma(t)$ is continuous, one can then define a critical exponent γ (by definition $\gamma > 1$)

$$\mathcal{A}_\Sigma(t) - \mathcal{A}_\Sigma^{(\text{eq})} \propto -(t_s - t)^\gamma . \quad (2.74)$$

The “critical” behavior around saturation can be obtained as follows. As $t \rightarrow t_s$, the tip of Γ_Σ approaches the null shell, i.e. $z_t - z_c \rightarrow 0$ with $z_t, z_c \rightarrow z_b$ (this is depicted by point D in Fig. 2-2 and Fig. 2-3(c)). Thus one can expand both $t - t_s$ and $\mathcal{A} - \mathcal{A}_{\text{eq}}$ in small $z_t - z_c$.

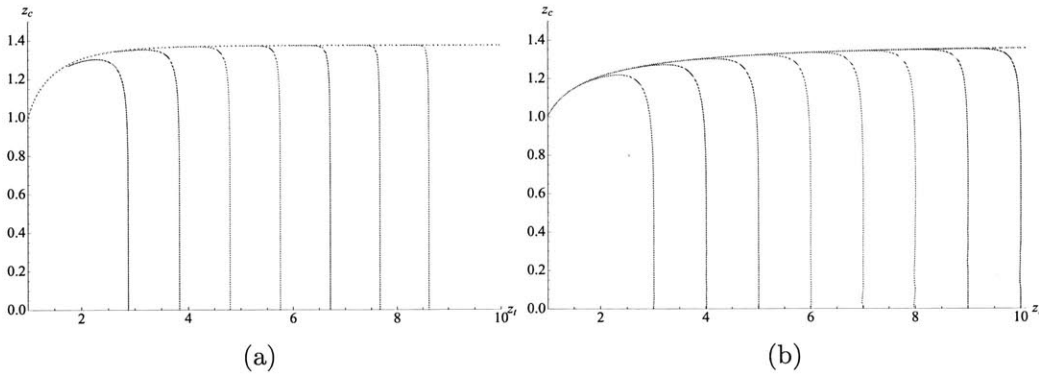


Figure 2-4: Parametric curves $(z_t(R, t), z_c(R, t))$ at fixed R and varying t for Schwarzschild $h(z)$ in $d = 3$. Different curves correspond to $R = 2, 3, \dots, 10$. In both plots, we choose units so that the horizon is at $z_h = 1$. (a): For a strip. Note the saturation is discontinuous with z_c lying behind the horizon at the saturation point where each curve stops. (b): For a sphere. The saturation is continuous and z_c lies outside the horizon at the saturation point (in the plot it is too close to the horizon to be discerned).

So far we have based our discussion on generic features of bulk extremal surfaces without referring to explicit solutions. To understand what happens during intermediate stages of time evolution, i.e. between B and C in the figures of Fig. 2-2, it is useful to work out specific examples of the evolution of $(z_t(R, t), v_t(R, t))$. In Fig. 2-4, we give the parametric plots of $(z_t(R, t), z_c(R, t))$ for various values of R , for Σ a strip and a sphere, for Schwarzschild $h(z)$ with $d = 3$. From these plots we see a

remarkable phenomenon: curves of varying R , after a brief period of order $O(z_h)$, all collapse into a single curve $z_c^*(z_t)$ highlighted by the dashed line in each plot.

In Sec. 2.3, we will show that the universal curve $z_c^*(z_t)$ corresponds to a critical line in (z_t, z_c) space: for a given z_t , Γ_Σ reaches the boundary only for $z_c < z_c^*$. In particular, for a Γ_Σ with $z_c = z_c^*(z_t)$, to which we will refer as a “critical extremal surface,” the surface stretches to $\rho, v = \infty$. As a consequence, for sufficiently large R and \mathfrak{t} , (z_t, z_c) lies very close to the critical line, and the evolution of $\mathcal{A}(R, \mathfrak{t})$ is largely governed by properties of the critical extremal surfaces. We will show that this is responsible for the linear growth discussed in [49].

To conclude this section we comment on the role of z_h in the evolution. As can be seen from the above discussion, z_h plays the characteristic scale for the evolution of Γ_Σ . There is an important geometric distinction between the time evolution of surfaces with $R \lesssim z_h$ and of those with $R \gg z_h$. In the former case, $\Gamma_\Sigma(\mathfrak{t})$ stays outside the horizon during its entire evolution, while in the latter case important parts of its evolution are controlled by the geometry near and behind the horizon. This supports the identification of z_h as a “local equilibrium scale” as only after such time scale does an extremal surface start probing the geometry around the black hole horizon.

2.3 Linear growth

In this section, we show that with Σ given by a strip $\mathcal{A}(R, \mathfrak{t})$ grows linearly with \mathfrak{t} for $R \gg \mathfrak{t} \gg z_h$. We will see that the evolution is largely controlled by the critical extremal surface discussed in the last section. The same growth also applies to a sphere and other shapes.

2.3.1 Linear growth

To obtain the behavior for $R \gg \mathfrak{t} \gg z_h$, we consider z_c close to z_c^* for some z_t ,

$$z_c = z_c^*(1 - \epsilon), \quad \epsilon \ll 1 \tag{2.75}$$

and assume that

$$\frac{z_c^*}{z_t}, \frac{z_m}{z_t} \ll 1, \quad \frac{z_c^*}{|\log \epsilon|} \ll 1. \quad (2.76)$$

In this regime we can expand \mathfrak{t} , R , and \mathcal{A} in a double expansion of $1/z_t$ and ϵ .

We now proceed to evaluate the boundary quantities \mathfrak{t} , R , and \mathcal{A} using (2.49)–(2.53). Note that these equations should be modified when $z(x)$ is not monotonic, which happens, for example, for $z_t > z_t^{(s)}$. Then $z_c \approx z_c^* < z_m$, i.e. after intersecting the shell, $z(x)$ first moves to larger values of z before turning around. In this case equation (2.49) should be modified to

$$R = \int_{z_c}^{z_t} dz \frac{1}{\sqrt{\frac{z_t^{2n}}{z^{2n}} - 1}} + \left(\int_{z_c}^{z_r} dz + \int_0^{z_r} dz \right) \frac{1}{\sqrt{H(z)}} \quad (2.77)$$

and similarly for others. In the above equation z_r is the root of $H(z)$ which is slightly smaller than z_m and $z_r = z_m$ for $\epsilon = 0$.

It is useful to separate $z(x)$ into four regions: (i) AdS region from z_t to z_c , (ii) from z_c to near z_m , (iii) running along z_m , and (iv) from near z_m to boundary $z = 0$. One can then check that contributions to \mathfrak{t} , R , and $\mathcal{A} - \mathcal{A}_{\text{vac}}$ from regions (ii) and (iv) are at most $O(z_c^*)$.³

Now let us look at region (iii). Near $z = z_m$, with $z_c = z_c^*(1 - \epsilon)$, we have

$$H(z) = H_2(z - z_m)^2 + b\epsilon, \quad (2.78)$$

where

$$H_2 = \frac{1}{2}H''(z_m), \quad b = -z_c^* \left. \frac{dE^2}{dz_c} \right|_{z_c^*}. \quad (2.79)$$

Note $H_2 > 0$ and that $b < 0$ ($b > 0$) for $z_t > z_t^{(s)}$ ($z_t < z_t^{(s)}$). In (2.50) (or its non-monotonic version), there is no contribution from region (i), while region (iii)

³When $z_m \rightarrow \infty$ as $z_t \rightarrow \infty$, one has to be careful because the integration range from z_c^* to z_m is large. One can check that divergent contributions from (ii) and (iv) cancel.

contributes at order $\log \epsilon$, leading to

$$\mathfrak{t} = -\frac{E(z_c^*)}{h(z_m)\sqrt{H_2}} \log \epsilon + \dots \quad (2.80)$$

In (2.49) (or (2.77)) there is an $O(z_t)$ contribution from (i) in addition to a $\log \epsilon$ term from (iii),

$$R = a_n z_t - \frac{1}{\sqrt{H_2}} \log \epsilon + \dots \quad (2.81)$$

where a_n was introduced (2.21) (c.f. (2.71)). Using (2.80), we can then rewrite (2.81) as

$$z_t = \frac{1}{a_n} \left(R - \frac{h(z_m)}{E(z_c^*)} \mathfrak{t} \right) + \dots \quad (2.82)$$

Now consider the evaluation of \mathcal{A} using (2.51)–(2.53). After subtracting the vacuum value \mathcal{A}_{vac} , the diverging contribution near $z = 0$ in region (iv) cancels and the dominant contribution is again from region (iii),

$$\frac{1}{\tilde{K}} \Delta \mathcal{A} = \frac{1}{\tilde{K}} (\mathcal{A} - \mathcal{A}_{\text{vac}}) = -\frac{z_t^n}{z_m^{2n} \sqrt{H_2}} \log \epsilon + O(1) \quad (2.83)$$

Collecting (2.80) and (2.83), we find

$$\Delta \mathcal{A} = \tilde{K} \lambda \mathfrak{t} + \dots \quad (2.84)$$

with

$$\lambda = \frac{z_t^n}{z_m^{2n}} \frac{h(z_m)}{E(z_c^*)} = \frac{\sqrt{-h(z_m)}}{z_m^n} + \dots \quad (2.85)$$

where in the second equality we have used (2.47) to express $E(z_c^*)$ as

$$E(z_c^*) = -\sqrt{-h(z_m) \left(\frac{z_t^{2n}}{z_m^{2n}} - 1 \right)} = -\sqrt{-h(z_m)} \frac{z_t^n}{z_m^n} + \dots \quad (2.86)$$

Upon substituting the explicit form of \tilde{K} (2.34), we have

$$\Delta \mathcal{A} = \sqrt{-\gamma(z_m)} A_{\text{strip}} \mathfrak{t} + \dots \quad (2.87)$$

where $\gamma(z_m)$ is the determinant of the induced metric on the critical extremal surface at z_m , which is spanned by v and x_2, \dots, x_n , i.e. directions along Σ . Using the equilibrium “density” \mathbf{a}_{eq} introduced in (2.27), we can also write (2.84) as

$$\Delta\mathcal{A} = \mathbf{a}_{\text{eq}} A_{\text{strip}} v_n \mathbf{t} + O(1) \quad (2.88)$$

where the velocity v_n is given by

$$v_n = \left(\frac{z_h}{z_m} \right)^n \sqrt{-h(z_m)}. \quad (2.89)$$

In particular, for $n = d - 1$, we have the entanglement entropy

$$\Delta S = \frac{\Delta\mathcal{A}}{4G_N} = s_{\text{eq}} A_{\text{strip}} v_E \mathbf{t} + O(1) \quad (2.90)$$

where s_{eq} is the equilibrium entropy density in (2.10), and

$$v_E \equiv v_{d-1} = \left(\frac{z_h}{z_m} \right)^{d-1} \sqrt{-h(z_m)}. \quad (2.91)$$

In the regime of (2.76) we can approximate the value of z_m in various equations above by that at $z_t = \infty$. So to leading order in large R limit, the evolution is linear. Note in order for (2.76) to be satisfied we need \mathbf{t} to be large enough so that z_c is sufficiently close to z_c^* , but not too large such that z_t becomes comparable to z_c^* (see (2.82)) to invalidate (2.76).

2.3.2 Example: Schwarzschild

Let us now consider the Schwarzschild case for explicit illustration. Depending on the value of $\eta = \frac{2n}{d}$, z_c^* and z_m behave differently in the limit of a large z_t . Below we consider these situations separately. While we are considering Schwarzschild, the discussion only depends whether z_c^* and z_m have a finite limit as $z_t \rightarrow \infty$. So we will still keep $h(z)$ general in our discussion.

$\eta > 1$

For $\eta > 1$, which covers the case of entanglement entropy $n = d - 1$ in $d > 2$, both z_c^* and z_m remain finite of order $O(z_h)$ in the limit of large z_t . The assumptions (2.76) then apply when $R \gg t \gg O(z_h)$.

In this case we can show that the linear growth (2.88) in fact persists all the way to saturation, which happens via a discontinuous transition. We do this by assuming the conclusion, strongly suggested by Fig. 2-4, and checking self-consistency.

With the linear growth (2.88), \mathcal{A} will reach its equilibrium value (2.27) at time

$$t_s = \frac{R}{v_n} = \frac{R}{\left(\frac{z_h}{z_m}\right)^n \sqrt{-h(z_m)}}, \quad (2.92)$$

when, from (2.82) and (2.86),

$$z_t = \frac{R}{a_n} \left(1 - \left(\frac{z_m^2}{z_t z_h}\right)^n\right) + \dots . \quad (2.93)$$

For $\eta > 1$ the second term in parentheses is small for large z_t , so we find that when the system reaches the equilibrium value, z_t is still very large.

When t is greater than (2.92), equation (2.88) exceeds its equilibrium value, and the extremal surface with smallest area is no longer a near-critical extremal surface to which (2.88) applies, but one that lies solely in the black hole region. Thus the extremal surface jumps at t_s , and the saturation is discontinuous. Note that for entanglement entropy, the saturation time is

$$t_s = \frac{R}{v_E} \quad (2.94)$$

where v_E was given in (2.91).

$\eta = 1$

For $\eta = 1$ and that of a spacelike Wilson loop in $d = 4$, z_c^* remains finite but z_m increases with z_t in the large z_t limit. In this case, there is still a linear regime, with

$$v_n = 1 . \tag{2.95}$$

Furthermore, the expression inside parentheses in (2.93) becomes zero at the time (2.92), i.e. z_t becomes comparable to z_c before (2.92) is reached. Thus the system exits the linear growth regime before saturation.

$\eta < 1$

For $\eta < 1$, both $z_c^* \sim z_t^\alpha$ (with $\alpha < 1$) and $z_m \propto z_t$ grow with z_t in the limit $z_t \rightarrow \infty$. Then since z_c^* is also very large for large z_t , it may take a long time for z_c to reach z_c^* . If z_t is still $O(R)$ as z_c first approaches z_c^* , the linear regime could still exist. Supposing such a regime exists, equation (2.89) gives for Schwarzschild $h(z)$

$$v_n^{(S)} = \left(\frac{z_m}{z_h} \right)^{\frac{d}{2}-n} \rightarrow \infty , \tag{2.96}$$

which is physically unreasonable and suggests that a linear regime does not exist. Explicit numerical calculation appears to be consistent with this expectation.

Next we generalize the linear growth found for a strip to general shapes. We show that for \mathfrak{t} in the range $R \gg \mathfrak{t} \gg z_h$, $\mathcal{A}_\Sigma(\mathfrak{t})$ generically exhibits linear growth in \mathfrak{t} with a slope independent of the shape of Σ . Again the technical requirement is that z_c^* should remain finite as $z_t \rightarrow \infty$, which for Schwarzschild $g(z)$ amounts to $2n \geq d$.

We first rederive the linear growth from a scaling limit, which we can extend straightforwardly to general shapes. We will also extend results to the wider class of metrics (2.16).

2.3.3 A scaling limit

The linear growth of the last section occurs when z_t is large but z_c^* remains finite in the limit $z_t \rightarrow \infty$. In this regime, with $z_c \approx z_c^*$ we have (from (2.41))

$$x_c = x(z_c) = a_n z_t - \frac{z_c^{n+1}}{n z_t^n} + \dots . \quad (2.97)$$

Also from (2.82) and (2.86)

$$a_n z_t = R - O(z_t^{-n}) . \quad (2.98)$$

The above equations suggest that in the black hole region we should consider a scaling coordinate

$$y = (R - x) z_t^n . \quad (2.99)$$

Indeed, in terms of y equation (2.47) has a scaling form independent of z_t to leading order as $z_t \rightarrow \infty$,

$$\left(\frac{dz}{dy}\right)^2 = \frac{h(z)}{z^{2n}} + a^2, \quad a^2 = \frac{g_c^2}{4z_c^{2n}} . \quad (2.100)$$

Similarly, to leading order in $1/z_t$, equation (2.48) becomes

$$\frac{dv}{dz} = \frac{1}{h} \left(\frac{a}{\sqrt{\frac{h(z)}{z^{2n}} + a^2}} - 1 \right) . \quad (2.101)$$

From (2.100) and (2.101), we conclude

$$\frac{dx}{dz} \sim \frac{1}{z_t^n}, \quad \frac{dv}{dz} \sim O(1) . \quad (2.102)$$

Then using z as the independent variable, the action (2.33) in the black hole region is

$$\mathcal{A}_{\text{BH}} = L^n A_{\text{strip}} \int_0^{z_c} dz \frac{1}{z^n} \sqrt{\left(\frac{dx}{dz}\right)^2 - 2\frac{dv}{dz} - h\left(\frac{dv}{dz}\right)^2}$$

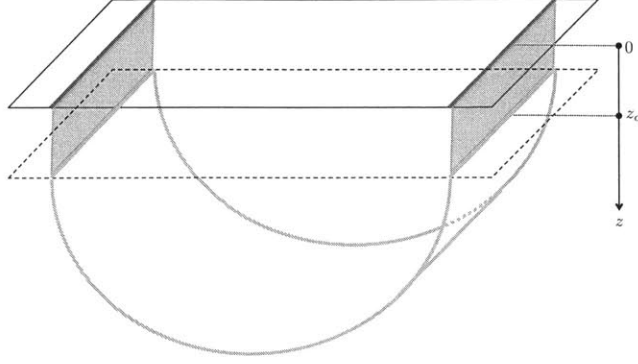


Figure 2-5: In the limit of a large z_t and a finite $z_c \approx z_c^*$, the evolution in the black hole region is essentially solely in the time direction, with two sides of the strip evolving independently.

$$= L^n A_{\text{strip}} \int_0^{z_c} dz \frac{1}{z^n} \sqrt{-2 \frac{dv}{dz} - h \left(\frac{dv}{dz} \right)^2} \quad (2.103)$$

where in the second equality we have dropped the term $\left(\frac{dx}{dz}\right)^2 \sim O(z_t^{-2n})$. It may look odd that in (2.103) $x(z)$ completely drops out. This in fact has a simple geometric interpretation: from (2.97)–(2.98), by the time the extremal surface reaches z_c , $x(z_c) = R - O(z_t^{-n})$ has essentially reached its boundary value R , while $v(z_c)$ is zero and still far away from its boundary value $v(z=0) = t$. Thus the evolution of the extremal surface in the black hole region (for $z < z_c$) is almost completely in the time direction. See Fig. 2-5 for an illustration. For purposes of calculating the area \mathcal{A} to leading order in $1/z_t$, we can simply ignore the evolution in x -direction. As a consistency check, we indeed recover (2.101) by variation of (2.103).

Integrating (2.101) we find that

$$t = \int_0^{z_c} \frac{dz}{h} \left(\frac{a}{\sqrt{\frac{h(z)}{z^{2n}} + a^2}} - 1 \right) \quad (2.104)$$

and further substituting (2.101) into (2.103) we have

$$\mathcal{A}_{\text{BH}} = L^n A_{\text{strip}} \int_0^{z_c} dz \frac{1}{z^{2n} \sqrt{\frac{h(z)}{z^{2n}} + a^2}} \quad (2.105)$$

The linear growth of $\mathcal{A}(t)$ can now be immediately understood from (2.104) and (2.105). As before, for $z_c = z_c^*$, $\frac{h(z)}{z^{2n}} + a^2$ has a double zero at its minimum z_m ⁴. For $z_c = z_c^*(1 - \epsilon)$ with $\epsilon \rightarrow 0$, both the integrals for t and \mathcal{A}_{BH} are then dominated by region around z_m , and we precisely recover (2.88).

Note that the action (2.103) as well as the linear growth of \mathcal{A} is in fact identical to that of [31], where entanglement entropy between half spaces lying on two asymptotic boundaries of an eternal AdS black hole was considered. The agreement can be easily understood from Fig. 2-5; in the large z_t limit, each half of the strip evolves independently in the black hole region solely in the time direction, which coincides with the set-up of [31].

2.3.4 General shapes

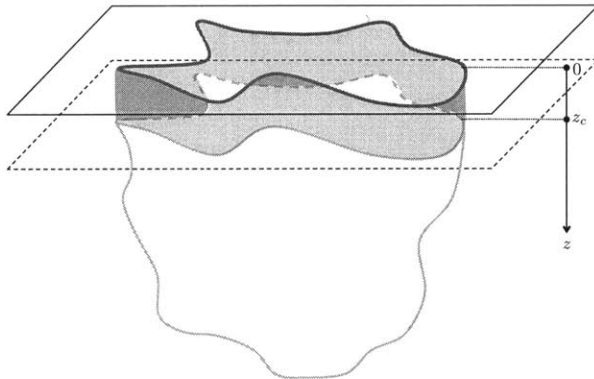


Figure 2-6: A cartoon of an extremal surface for Σ with some arbitrary shape, in the large size limit and t in the linear regime. Upon entering the black hole region, the extremal surface has essentially attained its boundary shape Σ . The evolution in the black hole region is essentially solely in the time direction and is the same as that for a strip.

The intuition obtained from the above discussion for a strip and Fig. 2-5 can now be generalized to arbitrary shapes. For arbitrary Σ , we again expect that in the limit $R \gg t \gg z_h$, the evolution of the extremal surface after entering the shell will be essentially solely in the time direction, as indicated in Fig. 2-6. In other words, in

⁴ $\frac{h(z)}{z^{2n}} + a^2$ differs from $H(z)$ only by an overall scaling and thus has the same minimum and zero.

the large size limit, when z_c is much smaller than the size of Σ , the curvature of Σ should not matter in the black hole and each point of the extremal surface essentially evolves like one on a strip. Below we present arguments that this is indeed the case.

Consider a smooth entangling surface Σ which can be parameterized in terms of polar coordinates as

$$\rho = Rr(\Omega), \quad x_a = 0 \quad (2.106)$$

where Ω denotes collectively the angular coordinates parameterizing Σ , R is the size of Σ , and the function $r(\Omega)$ specifies the shape of Σ . The bulk extremal surface can then be parameterized in terms of $\rho(z, \Omega), v(z, \Omega)$ with boundary conditions

$$\rho(z = 0, \Omega) = Rr(\Omega), \quad v(z = 0, \Omega) = t \quad (2.107)$$

and regularity at the tip of the surface.

Writing

$$d\Omega_{n-1}^2 = \sum_i g_i(\Omega) d\theta_i^2, \quad d^{n-1}\Omega = \prod_i \sqrt{g_i} d\theta_i \quad (2.108)$$

the area of Σ can be written as

$$A_\Sigma = R^{n-1} \int d^{n-1}\Omega r^{n-1}(\Omega) \sqrt{1 + \frac{1}{r^2} \sum_i \frac{r_i^2}{g_i}} \quad (2.109)$$

where

$$r_i \equiv \partial_{\theta_i} r(\Omega). \quad (2.110)$$

Meanwhile, in the Vaidya geometry, the action for an n -dimensional extremal surface ending on the above Σ can be written as

$$\mathcal{A}_\Sigma = L^n \int_\delta^{z_t} dz \int d^{n-1}\Omega \frac{\rho^{n-1}}{z^n} \sqrt{Q} \quad (2.111)$$

with

$$Q = \rho'^2 - 2v' - f(v, z)v'^2 + \frac{1}{\rho^2} \sum_i \frac{1}{g_i} G_i - \frac{1}{\rho^4} \sum_{i,j} \frac{(\rho_i v_j - \rho_j v_i)^2}{g_i g_j} \quad (2.112)$$

where we have used the notation

$$\rho' \equiv \partial_z \rho, \quad \rho_i \equiv \partial_i \rho, \quad v' \equiv \partial_z v, \quad v_i \equiv \partial_i v \quad (2.113)$$

and

$$G_i = -f(v, z)(\rho' v_i - \rho_i v')^2 + 2\rho_i(\rho' v_i - \rho_i v') - v_i^2. \quad (2.114)$$

In (2.111) δ is a short-distance cutoff. It is readily found that in the black hole region ρ and v have the following small z expansion (for $z \ll z_h$)

$$\rho(z, \Omega) = Rr(\Omega) - \frac{z^2}{R}\tilde{r}(\Omega) + \dots \quad (2.115)$$

$$v(z, \Omega) = t - z + O(z^{n+1}) \quad (2.116)$$

where $\tilde{r}(\Omega)$ is a function which can be determined from $r(\Omega)$.

For $R \gg t$, to leading order in $1/R$, the part of the extremal surface in the AdS region can be approximated by that in pure AdS, which we denote $\rho^{(0)}(z, \Omega)$ (and for which t constant). For $z/R \ll 1$, $\rho^{(0)}$ has the expansion

$$\rho^{(0)}(z, \Omega) = Rr(\Omega) + O(R^{-1}) \quad (2.117)$$

Note that in contrast to (2.115) which applies only to $z \ll z_h$, due to the scaling symmetry of pure AdS and that Σ as defined in (2.106) has a scalable form, equation (2.117) in fact applies to any $z/R \ll 1$ and in particular $z \sim z_c \approx z_c^*$. Thus we conclude that when the extremal surface enters the shell at z_c ,

$$\rho(z_c, \Omega) = Rr(\Omega) - O(R^{-1}). \quad (2.118)$$

From (2.115)–(2.116) and (2.118), the extremal surface in the black hole region should then have the following scaling

$$\rho' \sim O(R^{-1}), \quad \rho_i \sim O(R), \quad v_i \sim O(R^{-1}), \quad v' \sim O(1). \quad (2.119)$$

Plugging in the above scaling into the action (2.111) we find that to leading order in $1/R$,

$$\begin{aligned}
\mathcal{A}_{\Sigma,\text{BH}} &= L^n R^{n-1} \int_{\delta}^{z_c} dz \int d^{n-1}\Omega r^{n-1}(\Omega) \\
&\quad \frac{1}{z^n} \sqrt{-2v' - hv'^2} \sqrt{1 + \frac{1}{r^2} \sum_i \frac{r_i^2}{g_i}} \\
&= L^n A_{\Sigma} \int_{\delta}^{z_c} \frac{dz}{z^n} \sqrt{-2v' - hv'^2}
\end{aligned} \tag{2.120}$$

which reduces to (2.103). In particular, all evolution in ρ and Ω directions have dropped out. Thus we conclude that (2.88) in fact applies to all shapes with A_{strip} replaced by A_{Σ} .

The above discussion encompasses the case of Σ being a sphere for which $r(\Omega) = 1$. In that case one can derive the above scaling limit explicitly from equations (2.56)–(2.57). In particular, the linear growth regime is controlled by the first plateau of the critical extremal surface as indicated in Fig. 2-7.

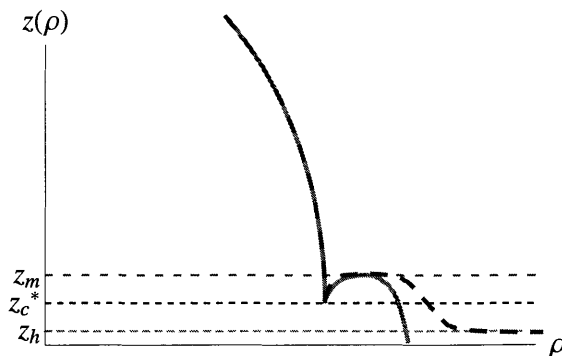


Figure 2-7: Cartoon: For a sphere, in the linear regime the extremal surface follows the critical extremal surface for a while but exits near the first plateau. The dashed curve is the critical extremal surface.

2.3.5 More general metrics

The above discussion can be readily extended to more general metrics of the form (2.16)–(2.18). The action (2.120) is replaced by

$$\mathcal{A}_{\text{BH}} = L^n A_\Sigma \int_0^{z_c} \frac{1}{z^n} \sqrt{-h(z)v'^2 - 2k(z)v'} , \quad (2.121)$$

from which $v(z)$ satisfies the equation

$$\frac{1}{z^n} \frac{hv' + k}{\sqrt{-hv'^2 - 2kv'}} = \text{const} \quad (2.122)$$

which can be solved as (b is a positive constant)

$$v' = \frac{k(z)}{h(z)} \left(\frac{b}{\sqrt{\frac{h(z)}{z^{2n}} + b^2}} - 1 \right) \quad (2.123)$$

with

$$\frac{d\mathcal{A}}{dz} = L^n A_\Sigma \frac{k(z)}{z^{2n}} \frac{1}{\sqrt{\frac{h(z)}{z^{2n}} + b^2}} . \quad (2.124)$$

Other than a prefactor $k(z)$ appearing in both equations, equations (2.123)–(2.124) are identical to (2.104)–(2.105). The constant b should be determined by matching conditions at the null shell, i.e. be expressible in terms of z_c alone in the limit $z_t \rightarrow \infty$. Its precise form is not important. As far as a z_c^* exists such that $\frac{h(z)}{z^{2n}} + b^2$ is zero at its minimum z_m , \mathcal{A} will have a linear growth regime for z_c close to z_c^* .

Since in the linear regime the leading behavior is given by the behavior of the RHS of (2.123)–(2.124) near z_m , the factor $k(z_m)$ cancels when we relate \mathcal{A} to \mathfrak{t} and we conclude \mathcal{A} is still given by (2.88) with the same v_n , i.e. the additional function $k(z)$ in (2.121) cannot be seen in the linear regime.

Chapter 3

The Gravity Duals of Entanglement Hamiltonians

3.1 Entanglement Hamiltonians

Given that the entanglement entropy of a spatial region is encoded in the gravity dual as the area of the minimal surface, one can ask if there is a simple interpretation in the bulk of the corresponding entanglement Hamiltonian operator

$$H = -\log \rho . \tag{3.1}$$

Note that the entanglement entropy suffers from UV divergences associated to short-distance entanglement across the boundary of the region. However, the claim that the relative entropy $\text{Tr}(\rho_2 \log \rho_2) - \text{Tr}(\rho_2 \log \rho_1)$ is regulator-independent [16, 53, 35] is equivalent to the statement that only the piece of H proportional to the identity operator is regulator-dependent. Then the UV divergences will not affect the modular evolution that we investigate.

Very few characterizations of a general entanglement Hamiltonian are known other than those which follow directly from its definition. For ρ associated to the causal completion¹ \mathcal{C} of some general spacetime region, H is a Hermitian and possibly un-

¹We define the causal completion of a set of points S in spacetime as the set of all points $\mathcal{C}(S)$

bounded operator acting on the Hilbert space of states in \mathcal{C} . The conjugation by H

$$\mathcal{O}(\alpha) = e^{i\alpha H} \mathcal{O} e^{-i\alpha H} \quad (3.2)$$

is an automorphism on $\mathcal{A}(\mathcal{C})$, the algebra of bounded operators in \mathcal{C} [29], and is a symmetry of the expectation value of all operators in \mathcal{C} ,

$$\text{Tr}(\rho \mathcal{O}(\alpha)) = \text{Tr}(\rho \mathcal{O}) . \quad (3.3)$$

In the special cases of the region being half-space in the Minkowski vacuum of any quantum field theory [8, 9] or conformally related configurations [17], and the case of the region being a null slab in the Minkowski vacuum of a CFT [11], H has been obtained explicitly and is a linear smearing of components of the energy-momentum tensor over the region. For a general region and state, however, little is known about H and one merely has the expectation that it cannot be written as a spacetime integral of local operators.

In this chapter, we consider the modular evolution of a quantum field theory density matrix ρ which has a semi-classical gravity dual,

$$\rho_\alpha \equiv e^{-i\alpha H} \rho e^{i\alpha H} , \quad (3.4)$$

where H is the entanglement Hamiltonian associated to the reduced density matrix of an arbitrary but fixed spatial region R ,

$$H = -\log \rho_R \otimes I . \quad (3.5)$$

Defined thus as an operator on the full Hilbert space, H is a non-smooth operator due to a kink at the boundary of R . However, integrating it over the location of R with respect to a smooth test function should result in a smooth operator. Furthermore, we will sometimes consider the operator $K = H_R - H_{\bar{R}}$, which we conjecture is a

such that all causal curves passing through each point also passes through S . In the literature $\mathcal{C}(S)$ is also called the domain of dependence or the causal development of S .

smooth operator. The logic is that the action of H very close to the boundary of R is very similar to that of the entanglement Hamiltonian associated to a half space in the Minkowski vacuum, for which K is a smooth operator.

The holographic duals of density matrices are not fully understood, and there is a related ongoing investigation of the possibility of formulating AdS/CFT for subregions [12, 13, 18, 37, 71, 32]. Moreover, the relation between entanglement and topology proposed in [51] would imply that knowledge of a density matrix is insufficient even to make probabilistic predictions for general bulk observables.² Thus although none of our results depend on ρ being pure, we will take ρ to be that of a pure state $|\psi\rangle$,

$$\rho = |\psi\rangle\langle\psi| \tag{3.6}$$

after which ρ_α is again a pure state,

$$\rho_\alpha = |\alpha\rangle\langle\alpha|, \quad |\alpha\rangle \equiv e^{-i\alpha H} |\psi\rangle. \tag{3.7}$$

Note that H is an example of a state-dependent operator. Somewhat analogously to [59, 60], we will find that there is a useful holographic interpretation of H when acting on states close to the reference state, in the sense that they are given by a small number of single-trace operators acting on $|\psi\rangle$.

We first show that at *linear order in α* , one can construct the classical metric g_α in the gravity dual of ρ_α to leading order in $1/N$, using the first law of entanglement entropy [10]

$$\delta\langle H\rangle = \delta S \tag{3.8}$$

and the minimal (RT) and extremal (HRT) surface prescriptions for calculating spatial entanglement entropy. Beyond linear order in α , we can use the fact that $H_\alpha = H$ to interpret the following expression for the metric perturbation (3.9) as a non-linear

²This is because information about entanglement is lost when a general probability distribution on the Hilbert space of quantum states is replaced by an associated density matrix $\rho = \sum_i p_i |\psi_i\rangle\langle\psi_i|$.

differential equation in α for the metric g_α . The metric perturbation takes the form

$$\partial_\alpha h = i \langle [H, \hat{h}] \rangle = \frac{1}{4G_N} i \langle [\hat{A}_h, \hat{h}] \rangle \quad (3.9)$$

where \hat{h} is a metric perturbation operator constructed by smearing boundary single-trace operators using bulk equations of motion,³ and \hat{A}_h is the change due to a metric perturbation h in the area of the extremal surface corresponding to R , obtained by elevating h to the operator \hat{h} . This equation should be interpreted in the linearized theory around the background dual to ρ , and the expectation values in (3.9) are taken with respect to ρ .

Given that expectation values of operators inserted solely in $\mathcal{C}(R)$ or in $\mathcal{C}(\bar{R})$ are invariant under modular evolution, if there is a bulk region $B(R)$ in $g \equiv g_0$ that is dual to ρ_R in the sense that the metric in $B(R)$ is determined by ρ_R , and similarly $B(\bar{R})$ for $\rho_{\bar{R}}$, the metric in those regions will be unchanged in g_α up to diffeomorphisms. Assuming the HRT prescription, the form of the ‘modular response’ $\partial_\alpha h$ in (3.9) implies that its diffeomorphism-invariant support is causal from the extremal surface of R - in other words, one can choose coordinates, at least patch-wise, such that the response vanishes at spacelike separation from the extremal surface. Thus the support is indeed absent from the ‘entanglement wedge’ advocated in [32] to be $B(R)$,⁴ the causal completion of the codimension-1 bulk region which interpolates between R and its extremal surface on a Cauchy slice. Parallel statements hold for \bar{R} .

Proceeding further and explicitly computing the diffeomorphism-invariant support of $\partial_\alpha h$ in simple examples, we find the following: except when R is a half-space or a sphere and ρ is the Minkowski vacuum of a CFT, in which case the support is causal from the *boundary* of the extremal surface,⁵ generically there is support on *interior* points of the extremal surface and thus at space-like separation from $\mathcal{C}(R)$ [71, 32]. Since H as a boundary operator is localized in $\mathcal{C}(R)$, this implies that generically the entanglement Hamiltonian is a ‘precursor’ [61] in the sense of being a boundary

³Such a construction of the metric perturbation operator in Poincaré AdS appeared in [33]. Also see [42].

⁴For other papers that have discussed how large $B(R)$ should be, see [13, 18, 37, 71].

⁵The same is true for conformally related configurations.

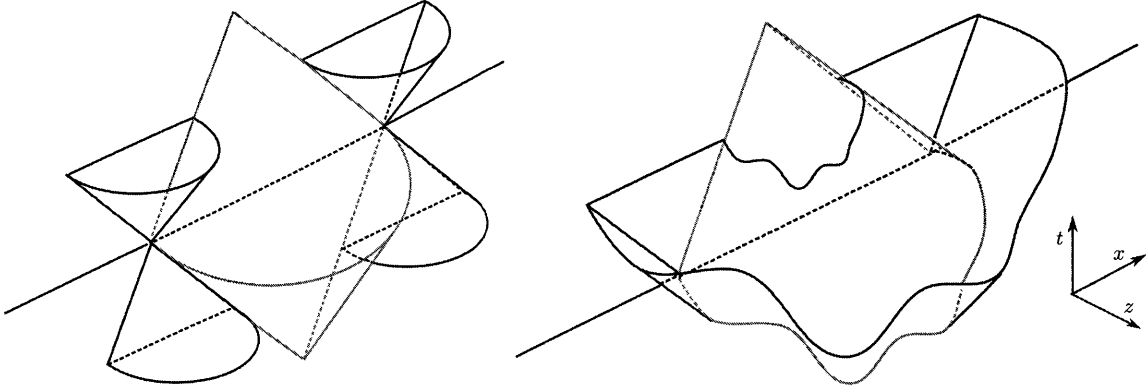


Figure 3-1: Cartoon of the diffeomorphism-invariant support of the modular response $\partial_\alpha h \approx (g_\alpha - g)/\alpha$, as computed using the HRT prescription. The entanglement wedge of R , whose intersection with the AdS boundary is $\mathcal{C}(R)$, is delineated in pink. Left: for configurations (ρ, R) with special symmetry, the response is causal from ∂R . Right: for generic (ρ, R) the response is causal from the entire extremal surface associated with R . To avoid clutter here we have only drawn the upper half of time evolution.

operator that is sensitive to bulk processes at space-like separation. Alternatively, the HRT prescription may need to be modified.

Moving beyond the metric, we discuss two methods of obtaining the deformation $\partial_\alpha \langle \mathcal{O}_1 \dots \mathcal{O}_n \rangle$ of n -point functions and other expectation values in general. The first is to utilize (3.8) and perform bulk computations of the change in entanglement entropy, staying in Lorentzian signature. The second is to analytically continue from Euclidean path integrals defined on replica sheets. In certain instances the Euclidean calculation simplifies further as we are able to use geometries with continuous conical deficit following [45]. The knowledge of n -point functions allows us to recover the action of the entanglement Hamiltonian on excitations about its defining state.

This chapter is organized as follows. In section 3.2, we study the modular response, or deformations of the metric and correlation functions in the linearized ρ_α state. We give an explicit construction of the metric deformation. We discuss methods of computing the deformation of general expectation values, and show that one can recover the action of the entanglement Hamiltonian on nearby excited states. We also examine the special symmetric case that R is a half-space and ρ is the Minkowski vacuum of a CFT. In section 3.3, we show that generically the modular response of the metric as computed using the HRT prescription violates bulk causality, and discuss

the known resolution of a similar conundrum for Wilson loops and geodesics. In section 3.4, we present conclusions and open questions. In the appendices we present computations of the metric response for an arbitrary region R when the gravity dual to ρ is the Poincaré AdS vacuum.

3.2 Modular response

3.2.1 Deformation of the metric

Let us fix a quantum field theory density matrix ρ and a spatial region R understood to be lying at some fixed time t_R . This defines an entanglement Hamiltonian

$$H_{\rho,R} = -\log \rho_R \otimes I, \quad \rho_R = \text{Tr}_{\bar{R}} \rho. \quad (3.10)$$

In defining the reduced density matrix ρ_R we assume that the Hilbert space factorizes as $\mathcal{H} = \mathcal{H}_R \otimes \mathcal{H}_{\bar{R}}$. The states in \mathcal{H}_R and $\mathcal{H}_{\bar{R}}$ live in the spacetime regions $\mathcal{C}(R)$ and $\mathcal{C}(\bar{R})$, respectively. The action of $H_{\rho,R}$ extends in the obvious way to the whole Hilbert space \mathcal{H} . From here on we omit the subscripts on $H_{\rho,R}$.

We start by making a simple observation as follows. Consider the unitary evolution of ρ by some Hermitian operator \mathcal{O} ,

$$\rho \rightarrow e^{-i\alpha\mathcal{O}} \rho e^{i\alpha\mathcal{O}}. \quad (3.11)$$

Working to linear order in α ,

$$\delta_{\mathcal{O}} \rho = i\alpha [\rho, \mathcal{O}]. \quad (3.12)$$

Then deforming ρ alternatively by the entanglement Hamiltonian H and another Hermitian operator \mathcal{O} ,

$$-\delta_H \langle \mathcal{O} \rangle = \delta_{\mathcal{O}} \langle H \rangle = \text{Tr}_R (\delta_{\mathcal{O}} \rho_R H) = \delta_{\mathcal{O}} S \quad (3.13)$$

where $S = -\text{Tr}_R(\rho_R \log \rho_R)$ is the entanglement entropy of region R . In the second equality we have used that H acts trivially on $\mathcal{H}_{\bar{R}}$ and the last equality is the first law of entanglement entropy.

The statements so far do not rely on gauge/gravity duality. Now let us assume ρ has a semi-classical gravity dual with classical metric g . Then we note that if the deformation $\delta_{\mathcal{O}}\rho$ again gives a semi-classical state, $\delta_{\mathcal{O}}S$ in (3.13) can be computed at leading order in $1/N$ using the HRT prescription. In particular, from the knowledge of $\delta_H \langle \mathcal{O} \rangle$ for single trace operators $\{\mathcal{O}\}$, we can construct the modular response $h \equiv \delta_H g$ as

$$\partial_\alpha h_{ab} = \frac{1}{\alpha} \delta_H \langle \hat{h}_{ab} \rangle = -\frac{1}{\alpha} \delta_{\hat{h}_{ab}} S = \frac{i}{4G_N} \left\langle \left[\hat{A}_h, \hat{h}_{ab} \right] \right\rangle \quad (3.14)$$

at leading order in $1/N$ or $O(1)$. Here \hat{h} is a metric perturbation operator written as a smearing of boundary single trace operators $\{\mathcal{O}\}$, by solving linearized equations of motion about the gravity dual of the original state ρ at leading order in $1/N$. When ρ is the vacuum, or dual to a matter-free solution of Einstein's equations, only the expectation value of the boundary energy-momentum tensor $\delta_H \langle T \rangle$ is non-vanishing at $O(N)$, so \hat{h} decouples from other bulk fields and is a smearing of T only. For generic states ρ , $\delta_H \langle \mathcal{O} \rangle$ is non-vanishing at $O(N)$ for $\mathcal{O} \neq T$ as well, and one has to solve a system of coupled differential equations for \hat{h} together with other bulk fields.

Meanwhile,

$$\hat{A}_h = \frac{1}{2} \int_E \gamma^{\alpha\beta} e_\alpha^a e_\beta^b \hat{h}_{ab} \quad (3.15)$$

is the change due to a metric perturbation h in the area of the extremal surface which ends on ∂R , elevated to an operator. The integral is over the extremal surface E in the unperturbed metric g , and we have denoted the induced metric and tangential vectors on E as $\gamma_{\alpha\beta}$ and e_α^a . Note that due to E being extremal, \hat{A}_h is a diffeomorphism-invariant operator. By causality in the bulk field theory, an operator $\hat{\phi}$ whose entire diffeomorphism-invariant description, or 'framing', is space-like to E , commutes with \hat{A}_h . Thus for instance, in the linearized theory, if one forms a curvature combination of the metric response $\partial_\alpha h_{ab}$ which transforms homogeneously under diffeomorphisms,

its support must be restricted to $\tilde{\mathcal{J}}(E)$,⁶ the causal future and past of E . Similarly, the modular response on the boundary corresponding to the leading fall-off of $\partial_\alpha h_{ab}$ will be restricted to the intersection of $\tilde{\mathcal{J}}(E)$ with the boundary, or $\mathcal{J}(\partial R)$ [32], as required by (3.3) and triviality of the action of H on $\mathcal{C}(\bar{R})$. We are able to check this explicitly for general regions R when g is Poincaré AdS.

Note that in the above the HRT prescription is put to use even when g is a static metric - we used extremal surfaces in the bulk to compute the entanglement entropy in the presence of time-dependent perturbations on top of g . Furthermore, the RHS of (3.14) can only give the piece of the response at absolute leading order in $1/N$, as it was derived using the leading order expression for S . In it \hat{h}_{ab} can be replaced with any boundary operator, but the leading order piece it yields will be zero for instance for multi-trace operators, and in the vacuum, single-trace operators other than T as well.

3.2.2 Deformation of general expectation values

In order to compute the deformation of general expectation values $\delta_H \langle \mathcal{O} \rangle = \alpha \partial_\alpha \langle \mathcal{O} \rangle$ (now \mathcal{O} can be any operator, for instance a Wilson loop or a string of single-trace operators) which are $O(1)$ or smaller using the RHS of (3.13), one has to reckon with quantum corrections to the RT/HRT prescriptions such as were considered in [23, 20].

However, if $|\psi\rangle$ is a time-symmetric state that can be obtained from a real Euclidean path integral with a corresponding classical gravity dual, one can derive the deformation of expectation values of operators in $|\alpha\rangle$ in another way.

Consider a Euclidean QFT path integral on a space with boundary at $t = 0$, with sources for single trace operators turned on. This defines a quantum state at $t = 0$ whose gravity dual is the analytic continuation to Lorentzian signature, of the Euclidean bulk field and metric configuration with AdS boundary conditions determined by the sources.

The trace $Z_k \equiv \text{Tr}(\rho_R^k)$ is given by the normalized QFT partition function on the

⁶We distinguish a causal domain in the bulk as opposed the boundary by placing a tilde above the character.

k -sheeted covering space branched over ∂R . In the bulk, the leading classical saddle is smooth in the interior and asymptotes to the k -sheeted AdS boundary geometry. As an operator, $\rho_R^k \otimes I$ is given by the Euclidean path integral from $t = 0$ that does nothing in \bar{R} and glues in the k sheeted region over R , see figure 3-2.

Therefore $\langle \psi | \mathcal{O}(x) (\rho_R^k \otimes I) | \psi \rangle$ for any operator \mathcal{O} is given by the associated Euclidean expectation value, $Z_{k+1}(\mathcal{O}(x)) / Z_{k+1}$. The operator ordering is determined by the Euclidean time of x relative to $\tau = it = 0$. Analytically extrapolating in $n = k + 1$ and continuing x to Lorentzian signature, one finds that⁷

$$\lim_{n \rightarrow 1} \partial_n \left(\frac{Z_n(\mathcal{O}(x))}{Z_n} \right) = - \langle \mathcal{O}(x) H \rangle. \quad (3.16)$$

The commutator response is given by the difference between the two operator orderings,

$$\partial_\alpha \langle \mathcal{O}(\vec{x}, t) \rangle = i \langle [H, \mathcal{O}(\vec{x}, t)] \rangle = \lim_{\varepsilon \rightarrow 0} \lim_{n \rightarrow 1} i \partial_n \left(\frac{Z_n(\mathcal{O}(\vec{x}, t - i\varepsilon))}{Z_n} - \frac{Z_n(\mathcal{O}(\vec{x}, t + i\varepsilon))}{Z_n} \right). \quad (3.17)$$

Note that the RHS is continued from Euclidean signature and only non-analyticities in $Z_n(\mathcal{O}(\vec{x}, \tau))$ contribute, which only exist for $\vec{x} \in R$, $\tau = 0$. Also note that for a time-symmetric state $|\psi\rangle$, one could in principle compare the value of some $\partial_\alpha \langle \mathcal{O} \rangle$ that is $O(N)$ as computed from the above with that from the Lorentzian method,

⁷The same equation but formulated using a twist operator appeared in [39].

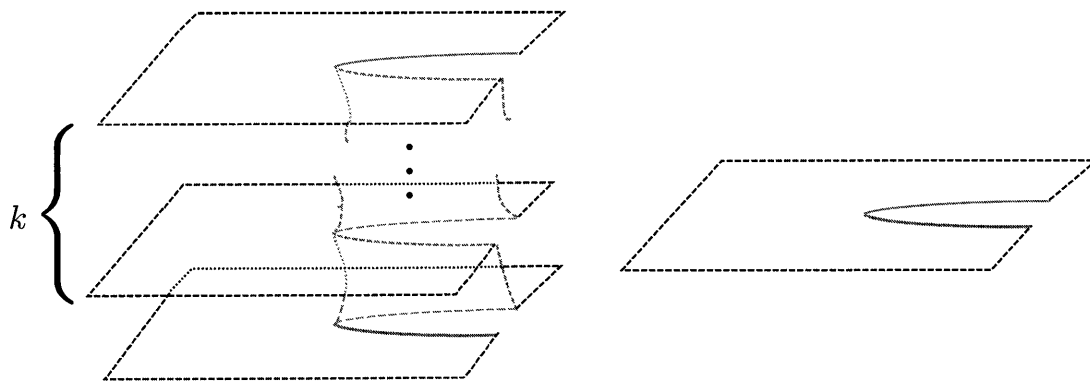


Figure 3-2: Riemannian sheets for Euclidean path integrals corresponding to the operator $\rho_R^k \otimes I$, left, and ρ_R , right.

and this would constitute a check of the HRT prescription.

As explained in [45], one can quotient the bulk saddle dual to Z_n by its replica symmetry, to obtain a geometry which asymptotes to the original single-sheeted AdS boundary but has a conical opening angle of $2\pi/n$ along a bulk defect. If the Euclidean expectation value in (3.16) is dominated by the classical bulk geometry, it can be extracted from the quotient space, and the analytic extrapolation in n is straightforward. This is the case when \mathcal{O} is a single-trace operator or some other operator whose expectation value in the large- N limit is given by a minimal geodesic or surface in the Euclidean bulk saddle.⁸

Then immediately from (3.17) we have

$$\partial_\alpha \langle \mathcal{O}(\vec{x}, t) \rangle = \lim_{\varepsilon \rightarrow 0} i \partial_\kappa \left(\frac{Z_\kappa(\mathcal{O}(\vec{x}, t - i\varepsilon))}{Z_\kappa} - \frac{Z_\kappa(\mathcal{O}(\vec{x}, t + i\varepsilon))}{Z_\kappa} \right) \Big|_{\kappa=0}, \quad (3.18)$$

where the RHS is continued from Euclidean signature with Z_κ being the partition function over conical defect geometries with opening angle $2\pi(1 - \kappa)$. This is particularly useful in computing the deformation of 2-point functions of high-dimension scalar operators, since the expectation values involved are given at leading order in terms of lengths of geodesics in classical saddles g_κ of Z_κ .

Finally, we note that the two methods outlined above translate to respective arguments that $|\alpha\rangle$ with α infinitesimal is indeed a semi-classical state with a gravity dual if $|\psi\rangle$ is. One needs to check that corrections to an n -point function of single-trace operators $\langle \mathcal{O}_1 \dots \mathcal{O}_n \rangle_\alpha$ besides the classical value $\langle \mathcal{O}_1 \rangle_\alpha \dots \langle \mathcal{O}_n \rangle_\alpha$ are subleading in $1/N$. Below we also find it instructive to explicitly identify the subleading corrections in the Lorentzian method.

Using (3.13), we have $\partial_\alpha \langle \mathcal{O}_1 \mathcal{O}_2 \rangle = -\alpha^{-1} \delta_{\mathcal{O}_1 \mathcal{O}_2} S$. For small α , the state $e^{i\alpha \mathcal{O}_1 \mathcal{O}_2} |\psi\rangle$ is described by the same classical metric in the bulk dual as $|\psi\rangle$ to leading order in $1/N$, and thus δS vanishes at leading order. At subleading order, there are two sources of contributions to δS - corrections to the bulk metric, and subleading corrections to S besides the extremal area. The former arises from the bulk tree-level diagram of two

⁸[64] suggested that general correlation functions of H with operators in Minkowski space are equivalent to correlation functions of just the operators on spacetimes with conical defects.

scalars and the metric, and is calculable from the bulk Lagrangian - in CFT language, the $T\mathcal{O}\mathcal{O}$ 3-point function gives a nonzero VEV to T in the state, and there is also an explicit $\mathcal{O}\mathcal{O}$ correction to the boundary expression for the bulk metric operator [41]. The latter corrections include the bulk scalar field entanglement entropy [23], so is more difficult to determine.

In any case, contributions from both are suppressed by $1/N$ compared to the classical, factorized 2-point function. The same reasoning applies to general n -point functions, and we have the desired conclusion.

Using (3.17), we reach an identical conclusion by noting that $Z_n(\mathcal{O}_1 \dots \mathcal{O}_n)$ obeys large- N factorization, due to the fact that a semi-classical bulk configuration dominates its gravity dual and n -point functions on the boundary are limits of bulk n -point functions.

3.2.3 Action of the entanglement Hamiltonian on excitations

It is interesting to determine if the action of the entanglement Hamiltonian on states other than its defining state also has a useful holographic description. For states that are dual to completely different geometries, we do not expect the action to be simple. However, for states that are made by acting with a small (compared to N) number of single-trace operators on $|\psi\rangle$, one can make some progress.

We would like to characterize states of the form $H\mathcal{O}|\psi\rangle$ where now \mathcal{O} again denotes a single-trace operator. This can be done by computing the inner products $\langle\psi|\mathcal{O}(x)[H, \mathcal{O}(y)]|\psi\rangle$. For general position x , this is difficult to determine. However in the special case that $x \in C(\bar{R})$, one can move the insertion of H such that it always acts on $|\psi\rangle$, and use the methods in the previous section to compute the result.

We know that H is not a smooth operator because of a kink at ∂R , but we conjecture that $K = H_R - H_{\bar{R}}$ is smooth. This is because the action of H on operators inserted very close to ∂R should be well approximated by the half-space result (3.20), for which K is explicitly a smooth operator. One can see that this approximation is valid from the Euclidean expressions (3.16) and (3.17). At sufficiently short distances ∂R may be approximated by a flat plane. Moreover, the expectation values of opera-

tors inserted sufficiently close to ∂R in the n -sheeted covering spaces are governed by short-distance physics and thus do not depend on the state. Finally, at least in our situation where the analytic continuation in n is simple in the gravitational dual, it is clear that the same is true with H replacing the branch point of the covering space.

For $y \in C(R)$, we have $[K, \mathcal{O}(y)] = [H, \mathcal{O}(y)]$ and thus $i\langle\psi|\mathcal{O}(x)[K, \mathcal{O}(y)]|\psi\rangle = \partial_\alpha\langle\alpha|\mathcal{O}(x)\mathcal{O}(y)|\alpha\rangle$. Then assuming that K is a smooth operator, we may determine the entire action of K on such states by analytic continuation of x from $C(\bar{R})$ to the entire spacetime.

In computing $\partial_\alpha\langle\alpha|\mathcal{O}(x)\mathcal{O}(y)|\alpha\rangle$, we saw in the previous section that there is a contribution that is difficult to determine in the Lorentzian method, the change in the bulk entanglement entropy. Thus here we restrict to $|\psi\rangle$ such that the Euclidean method can be applied, and consider the special case of high-dimension single-trace scalar operators, dual to heavy fields in the bulk (with mass parametrically larger than the AdS scale, but smaller than the Planck scale).

Then using (3.18) and the geodesic approximation $\langle\mathcal{O}(x)\mathcal{O}(y)\rangle_\kappa \propto e^{-ml(x,y,\kappa)}$, we have

$$\partial_\alpha\langle\mathcal{O}(x)\mathcal{O}(y)\rangle \approx \lim_{\varepsilon \rightarrow 0} -im \partial_\kappa (l(x, y_+, \kappa) - l(x, y_-, \kappa))|_{\kappa=0} \langle\mathcal{O}(x)\mathcal{O}(y)\rangle \quad (3.19)$$

where $l(x, y, \kappa)$ is the length of the geodesic of minimal length connecting points x and y in g_κ , and y_\pm are obtained by the replacements $t_y \rightarrow t_y \mp i\varepsilon$. The discontinuity in $l(x, y, \kappa)$ as y crosses R is due to the deficit angle about ∂R .

For a complete characterization of the action of H on excited states near $|\psi\rangle$, one needs to compute more general inner products $\langle\psi|\mathcal{O}(x_1)\dots\mathcal{O}(x_n)[H, \mathcal{O}(y_1)\dots\mathcal{O}(y_m)]|\psi\rangle$. Then modulo analytic continuation in x_i to the entire space-time, one could again take $x_i \in C(\bar{R})$, $y_i \in C(R)$, converting the problem to that of obtaining modular deformations of n -point functions. The latter can be computed in principle with the methods we have discussed, although the computations will be more difficult than in the simplest instance of (3.19).

3.2.4 A special symmetric case

Here we examine the modular response $\partial_\alpha h_{ab}$ as given by (3.14) in the simple case that ρ is the Minkowski vacuum of a d -dimensional CFT, and the spatial region R is half-space. The entanglement Hamiltonian H is known in this configuration [8, 9], and taking the half-space to be $x_1 > 0$ at $t_R = 0$, can be written as

$$H = 2\pi \int_{-\infty}^{\infty} d^{d-2}x_{\perp} \int_0^{\infty} dx_1 x_1 T_{tt}(t=0, \vec{x}) . \quad (3.20)$$

Given that H is a smearing of local operators on R , bulk-causality implies the diffeomorphism-invariant support of the modular response $\partial_\alpha h_{ab}$ must be causal from R . As we have argued above it is also causal from E , so in fact it should be causal from $R \cap E = \partial R$.⁹ See left in figure 3-1.

It is easy to check that indeed Einstein equations in Poincaré AdS conspire with the geometry of E in this case to make the integral over E

$$z^2 \partial_\alpha h_{\mu\nu} \propto \int_0^{\infty} dz' \int d^{d-2}x'_{\perp} z'^{1-d} G_{\mu\nu pp}(z, x; z', x') , \quad p = 2, \dots, d-1 \quad (3.21)$$

into a boundary term at $\partial E = \partial R$, where in the integrand a sum over p is implied. Here we are working in transverse-traceless and Fefferman-Graham gauge for h . For independent components $\partial_\alpha h_{ti}$ and $\partial_\alpha h_{ij}$ where i, j are spatial indices, we have the propagator components

$$\begin{aligned} G_{tipp} &= [-((d-1)\eta_{ip}\partial_t\partial_p - \partial_t\partial_i)\partial^2 + (d-2)\partial_t\partial_i\partial_p^2] G_4 , \\ G_{ijpp} &= [((d-1)\eta_{ip}\eta_{jp} - \eta_{ij})\partial^4 - ((d-1)(\eta_{jp}\partial_i\partial_p + \eta_{ip}\eta_j\eta_p) - \partial_i\partial_j - \eta_{ij}\partial_p^2)\partial^2 + (d-2)\partial_i\partial_j\partial_p^2] G \end{aligned} \quad (3.22)$$

and switching derivatives using $\partial_\mu G_4 = -\partial'_\mu G_4$, terms with a ∂_p integrate by parts

⁹A related result that appeared previously in the literature is the first law of black hole mechanics that the perturbed area of a stationary black hole horizon reduces to an integral of energy density over the boundary of the horizon [40]. In [22] the authors used the HRT prescription to translate the first law of entanglement entropy for balls in a CFT vacuum to a sub statement of the first law of black hole mechanics, and derived from it linearized Einstein equations.

over x'^p , and terms without a ∂_p integrate by parts over z' using the equation of motion

$$z'^{1-d}\partial'^2 G_4 = -\partial'_z (z'^{1-d}\partial'_z G_4) . \quad (3.23)$$

In particular, the linearized Weyl response $\partial_\alpha C_{abcd}$ associated to $\partial_\alpha h_{ab}$, which is homogeneous under diffeomorphisms about AdS , is manifestly causal from ∂R as kernels in the metric-Weyl propagator $W_{abcd;\rho\sigma}(z, x; z', x')$ are causal for $z \geq z'$.

From the metric response as computed in (3.21), one can reproduce the modular evolution of space-like two-point functions as effected by (3.20), as follows.

Consider the two point function of a primary scalar operator \mathcal{O} of dimension D , which in the CFT vacuum is up to a constant

$$\langle \mathcal{O}(x)\mathcal{O}(y) \rangle = \frac{1}{(x-y)^{2D}} . \quad (3.24)$$

The entanglement Hamiltonian (3.21) acts on any operator $\mathcal{O}(y)$ in the Rindler region $\mathcal{C}(R)$ as

$$e^{i\alpha H}\mathcal{O}(y)e^{-i\alpha H} = \mathcal{O}(y(\alpha)) , \quad (3.25)$$

$$y^\pm(\alpha) = y^\pm e^{\mp 2\pi\alpha} , \quad y^\pm = y^1 \pm y^0 , \quad (3.26)$$

and trivially on operators localized in the complementary Rindler region $\mathcal{C}(\bar{R})$. Thus if we choose $x \in \mathcal{C}(\bar{R})$ and $y \in \mathcal{C}(R)$,

$$\partial_\alpha \langle \mathcal{O}(x)\mathcal{O}(y) \rangle = 4\pi D \frac{y^0(x^1 - y^1) - y^1(x^0 - y^0)}{(x-y)^2} \langle \mathcal{O}(x)\mathcal{O}(y) \rangle . \quad (3.27)$$

Now, if the gravity dual of a boundary quantum field theory has metric g , and if g is the analytic continuation of a Euclidean geometry and possesses a natural vacuum, we expect that generically we will be able to approximate space-like two-point functions of scalar operators of large dimension in the boundary theory using geodesics in g [6, 50]. In the case at hand, the metric evolved in modular time g_α of Poincaré AdS g is a topological black hole up to an isometry in g [17]. Thus we expect

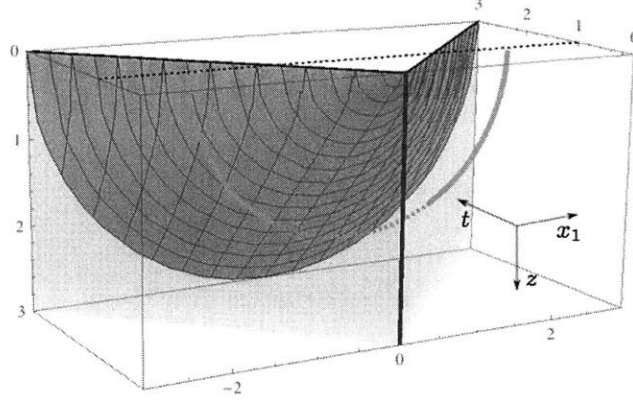


Figure 3-3: Depiction of a geodesic in Poincaré AdS which computes the expectation value of an equal-time two-point function $\langle \mathcal{O}(x)\mathcal{O}(y) \rangle$, with x and y in Rindler regions $\mathcal{C}(\bar{R})$ and $\mathcal{C}(R)$, where R is the half-space $x_1 \geq 0$. (Note we have $d = 2$ in the figure for ease of drawing, but all considerations here are in $d \geq 3$ for which there are local gravitational excitations in the bulk.) The light-cone and boundary light-cone from ∂R are shown in solid beige and transparent purple, respectively. The solid purple line is the extremal surface E . All contributions to $\partial_\alpha \langle \mathcal{O}(x)\mathcal{O}(y) \rangle$ come from the intersection of the geodesic with the boundary light-cone from ∂R .

the geodesic approximation to be valid, and for $D \gg 1$, to have up to a constant

$$\langle \mathcal{O}(x)\mathcal{O}(y) \rangle_\alpha \approx e^{-DL^{-1}l(x,y,\alpha)} \quad (3.28)$$

where L is the AdS radius and $l(x, y, \alpha)$ is the length of the geodesic of minimal length connecting space-like boundary points x and y in the metric g_α . It follows that (*c.f.* (3.19))

$$\partial_\alpha \langle \mathcal{O}(x)\mathcal{O}(y) \rangle \approx -\frac{D}{L} \partial_\alpha l(x, y, \alpha) \langle \mathcal{O}(x)\mathcal{O}(y) \rangle \quad (3.29)$$

and restricting ourselves to equal-time two-point functions without loss of generality - space-like two-point functions can be rotated in the $t - x_\perp$ dimensions to be brought to equal time without breaking the symmetry of our configuration - and comparing with (3.27), we would like to verify

$$\partial_\alpha l \approx 4\pi L \frac{t(x^1 - y^1)}{(\vec{x} - \vec{y})^2}, \quad t = x^0 = y^0. \quad (3.30)$$

Since the length of a geodesic is invariant under linear deformations, $\partial_\alpha l$ is given

by the change in length of the original geodesic in Poincaré AdS. The most general such geodesic at equal time is a semi-circle

$$z(w) = \sqrt{r^2 - w^2}, \quad x^k(w) = \frac{y^k + x^k}{2} + \frac{w}{r} \left(\frac{y^k - x^k}{2} \right), \quad k = 1, 2, \quad (3.31)$$

of radius $r = \sqrt{(y^1 - x^1)^2 + (y^2 - x^2)^2}/2$ parametrized by $-r \leq w \leq r$. One can check that enforcing $x \in \mathcal{C}(\bar{R})$ and $y \in \mathcal{C}(R)$, the geodesic never enters the light-cone from ∂R inside which the Weyl response $\partial_\alpha C_{abcd}$ is non-zero. See figure 3-3. A metric perturbation $\partial_\alpha h_{ab}$ whose Weyl response vanishes is locally a pure diffeomorphism, and such a perturbation, if smooth, cannot contribute to $\partial_\alpha l$ which is a diffeomorphism-invariant quantity much like (3.15). Thus $\partial_\alpha l$ is entirely due to the singular kink in the metric perturbation which exists on the boundary light-cone of ∂R in transverse-traceless and Fefferman-Graham gauge.

Integrating the metric perturbation (3.21) over the geodesic given in (3.31), we have

$$\begin{aligned} \partial_\alpha l &= -\frac{C_T \lambda_d^2 \kappa_d^2 L^d}{64 G_N} \frac{1}{r^3} I, \\ I &\equiv \int_{-r}^r dw \int_0^\infty dz' \int d^{d-2} x'_\perp z'^{1-d} \left((\Delta x^1)^2 G_{11pp} + (\Delta x^2)^2 G_{22pp} + 2\Delta x^1 \Delta x^2 G_{12pp} \right), \end{aligned} \quad (3.32)$$

where $\Delta x^k \equiv y^k - x^k$. Thus verifying (3.30) is equivalent to checking

$$I \propto t(y^1 - x^1)r \quad (3.33)$$

where the constant of proportionality only fixes the $O(N)$ constant C_T in the energy-momentum tensor two-point function appearing in $[T, T]$. The integral I simplifies after integrating by parts and using the equation of motion (3.23), but we still need to integrate numerically at a finite cutoff ε on light-cone singularities appearing in the bulk-to-bulk kernels G_s , as we have not isolated the analytic form of the singularities. We find precise agreement with (3.33) as shown for example in $d = 3$ in figure 3-4.

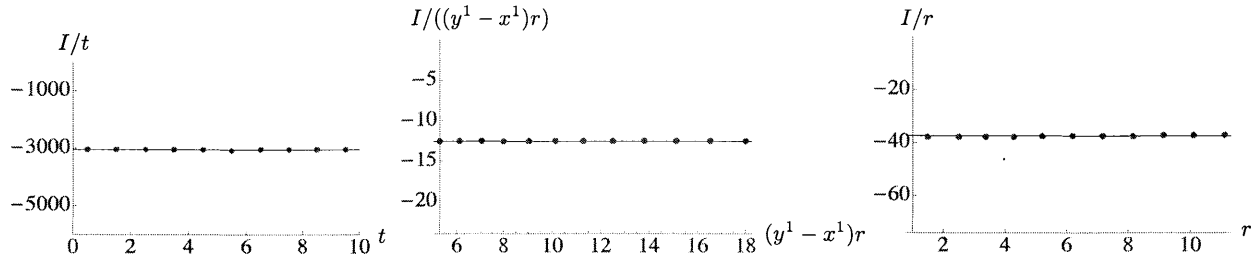


Figure 3-4: Tests of the scaling of I in (3.32) in $d = 3$ and at $\varepsilon = 10^{-3}$. The fixed parameters in each plot are as follows - left: $y^1 = -x^1 = 11$, $\Delta x^2 = 0$, center: $t = 1$, $x^1 = -3/2$, $\Delta x^2 = 0$, right: $t = 1$, $y^1 = -x^1 = 3/2$.

3.3 Propagation of metric response

We have seen that although the modular response of the metric $\partial_\alpha h$ (3.14) is naively an integral over the extremal surface E , and propagates in the bulk space-time g from the entirety of E , in the special case that ρ is the CFT vacuum in Minkowski space and R is half-space, it reduces to a boundary term at $\partial E = \partial R$. The same is true for conformally related configuration. As a consequence, the entanglement Hamiltonian H , which by definition is localized to the boundary spacetime region $\mathcal{C}(R)$, is seen to act locally in the bulk space-time g with $\partial_\alpha h$ propagating causally from $\partial R \in \mathcal{C}(R)$.

However, for a generic state ρ and region R , $\partial_\alpha h(x) \sim [H, \hat{h}(x)]$ is non-zero at space-time points x of g at which the entire operator $\hat{h}(x)$ in its bulk-local form, including its framing, is space-like to $\mathcal{C}(R)$.¹⁰ This can be seen, for instance, by considering general regions R in the case that g is Poincaré AdS. One can use the extremality of E to integrate by parts the integrand in $\partial_\alpha h$, but there is a genuine bulk integrand remaining that does not integrate to a boundary term. The same is true after acting with derivatives to obtain the Weyl response $\partial_\alpha C$, which measures the gauge-invariant support of $\partial_\alpha h$. In particular, the Weyl response is non-vanishing on points in the interior of E , which is guaranteed to be space-like from $\mathcal{C}(R)$ [71, 32]. In figure 3-5 we plot a component of the Weyl response on an interior point of E for an R which is a slab in $d = 3$.

¹⁰The need to consider the full diffeomorphism-invariant description of a bulk operator when considering issues of bulk locality was pointed out in [34].

The upshot is that assuming the HRT prescription of using extremal surfaces in Lorentzian spacetimes to calculate entanglement entropy, H for a generic state ρ and region R violates bulk locality at lowest order in the large N limit in which we expect the bulk to be described by an ordinary quantum field theory on a fixed background. The expectation value of H , which for linear perturbations measures the entanglement entropy of R with respect to \bar{R} in the boundary field theory, is sensitive to bulk perturbations that are space-like to the region on which H is supported.

Starting in [61], operators in the boundary theory whose expectation values are sensitive to space-like bulk perturbations so as to ensure that the boundary theory encodes all of the information - in the gravity dual in the context of gauge/gravity duality - have been called precursors. Using the naive saddle approximation and computing expectation values of Wilson loops with areas of extremal world-sheets in perturbed backgrounds, it would seem that Wilson loops are precursors [65] in complete analogy to the case of entanglement Hamiltonians that we have investigated, yet in [27] it was pointed out that such reasoning fails because the naive saddle is incorrect. In fact the same flawed reasoning would lead one to conclude that the two-point function of space-like operators in ordinary quantum field theory are sensitive to perturbations at space-like separation from both operators, in violation of locality. Similarly, Wilson loops are dual to extended string states, hence the locality and causality of perturbative string theory implies that such commutators must vanish. One can also understand that the extremal world-sheet approximation for expectation values of Wilson loops and the geodesic approximation for space-like two-point functions cannot be generally valid in Lorentzian signature, from the fact that the one-point function of the metric does not uniquely specify the state of the bulk quantum field theory [50].¹¹

Here we simply point to two possibilities. The first is that the HRT proposal is correct in which case we have shown that entanglement Hamiltonians associated to spatial regions are genuine precursors which differ qualitatively from possible pre-

¹¹In [24] it was shown that even in static black hole backgrounds one needs to take into account non-trivial complexified geodesics.

cursors as previously characterized in [25]. There it was proposed that *short-distance* properties of Wilson loops may be sensitive to bulk processes at space-like separation. However, the value of an entanglement Hamiltonian, for example at linear order, measures spatial entanglement which generically includes long-range entanglement. It follows that, again generically, at least part of the bulk information which is encoded acausally via the entanglement Hamiltonian is encoded in long-distance properties of the boundary state.¹² The second possibility is that the HRT proposal needs to be modified in a manner in which the state of the bulk quantum field theory is explicitly taken into account, and that with the correct computation of spatial entanglement entropy, corresponding entanglement Hamiltonians may not be precursors as seen in the large N limit.

3.4 Further directions

In this chapter, we have obtained descriptions in the gravity dual of the action of the entanglement Hamiltonian - associated to an arbitrary spatial region in a quantum field theory state that has a gravity dual - on its defining state and nearby states. This was possible after obtaining the deformation of expectation values, in particular n -point functions of single-trace operators, in the original state evolved unitarily with the entanglement Hamiltonian. The Lorentzian method of obtaining deformed expectation values relies on the first law of entanglement entropy, and at leading order in $1/N$, the RT and HRT prescriptions for computing entanglement entropy. We also discussed a Euclidean method that applies only in the case of certain time-symmetric states but does not rely on the HRT prescription, and thus could potentially be used to cross-check it.

Focusing on the metric deformation obtained using the Lorentzian method, we found that in special symmetric cases in which the entanglement Hamiltonian generates a diffeomorphism on a subset of the bulk space-time, the deformation propagates

¹²For example consider the response $\alpha \partial_\alpha C = -\delta_{\hat{C}} \langle H \rangle = -\delta_{\hat{C}} S$ for g Poincaré AdS and R an arbitrary region. For even d , the non-local part of the response sensitive to perturbations space-like to $C(R)$ includes a piece that is finite in the limit that the light-cone cutoff ε goes to zero.

causally from the boundary of the spatial region in the quantum field theory. That this reduction to the boundary does not occur generically, however, led us to the surprising statement that the action of a generic entanglement Hamiltonian does not respect bulk causality to lowest order in $1/N$, or in other words, that the entanglement Hamiltonian as an operator cannot be localized to $\mathcal{C}(R)$ to any finite order in perturbation theory.

That the interior points of generic HRT surfaces are not in causal contact with $\mathcal{C}(R)$ is actually crucial for it to be compatible with causality in the boundary quantum field theory [32]. Yet we found that it is precisely this feature that puts it at tension with causality in the low energy bulk quantum field theory. It is an interesting future direction to think about whether and how the HRT prescription could be modified to resolve this tension. We pointed out that any modification will likely have to do with incorporating the state of the bulk quantum field theory more explicitly.

It will also be interesting to explore whether we can obtain further characterizations of the action of generic entanglement Hamiltonians with the aid of methods we began developing in this chapter.

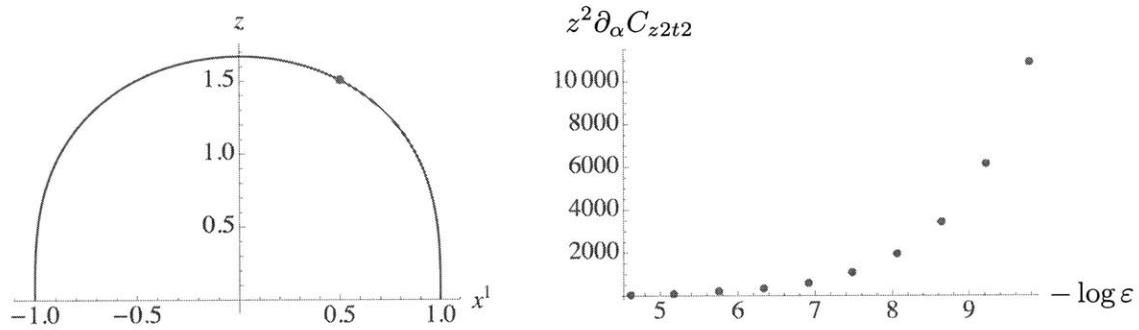


Figure 3-5: A component of the Weyl response on an interior point of E for an R which is a slab in $d = 3$ with finite extent $-1 \leq x^1 \leq 1$ and extending infinitely in remaining boundary spatial coordinate x^2 . Left: The point on E at which we measure the Weyl response. We show a $t = t_R$, $x^2 = \text{const.}$ cross section of the bulk space-time g which is Poincaré AdS. Right: The component $\partial_\alpha C_{z2t2}$ on the point specified as a function of the light-cone cutoff ε . It diverges as $\varepsilon \rightarrow 0$.

Chapter 4

Conclusions

We conclude by outlining directions for future research that could shed light on questions we discussed in the introduction, namely the emergence of local degrees of freedom in the bulk and a more direct derivation of gauge/gravity duality.

One is to look for a bulk interpretation of the entanglement first law $dS = d\langle H \rangle$ [10], for S the entanglement entropy of an *arbitrary* spatial region on the boundary. In the case that the region is a sphere and the state is the conformal vacuum, the bulk interpretation is given by Wald's first law of black hole mechanics, which equates the linearized change in black hole entropy to that of an energy that is defined at spatial infinity with respect to a Killing vector [40]. For an arbitrary region, the absence of a Killing vector and indeed any natural vector field which preserves asymptotically AdS boundary conditions, makes it quite challenging to find a suitable definition of energy that would enter a presumed bulk first law.

However, if such a bulk first law or equilibrium condition $dS = dE/T$, $T = \hbar$ can be formulated for a suitable energy E , and which pertains to extremal codimension-two surfaces in Einstein gravity, it would help establish a more explicit correspondence between AdS geometries and cMERA networks, where in the latter setting it is natural to think of the entanglement across a codimension-two surface as having been maximized when the surface is extremal [54, 55].

Another direction is to look for simple toy models which have a suitable notion of gravity dual and on which the cMERA procedure can be implemented analytically.

For instance, there exists a large- N matrix model of non-interacting fermionic degrees of freedom whose dual is given by dilatonic gravity coupled to a tachyon [44] and for which there is in principle no obstacle to implementing the cMERA procedure, due to the boundary theory being non-interacting. A more far-reaching goal is to implement the cMERA procedure on a model which has a black hole horizon in its gravity dual - a possible candidate is given by Kitaev's random quartic model of Majorana fermions, which he has shown possesses a kind of dual black hole horizon [43].

Bibliography

- [1] Javier Abajo-Arrastia, Joao Aparicio, and Esperanza Lopez. Holographic Evolution of Entanglement Entropy. *JHEP*, 1011:149, 2010.
- [2] Ofer Aharony, Oren Bergman, Daniel Louis Jafferis, and Juan Maldacena. N=6 superconformal Chern-Simons-matter theories, M2-branes and their gravity duals. *JHEP*, 0810:091, 2008.
- [3] Tameem Albash and Clifford V. Johnson. Evolution of Holographic Entanglement Entropy after Thermal and Electromagnetic Quenches. *New J.Phys.*, 13:045017, 2011.
- [4] Andrea Allais and Erik Tonni. Holographic evolution of the mutual information. *JHEP*, 1201:102, 2012.
- [5] Rudolf Baier, Stefan A. Stricker, Olli Taanila, and Alekski Vuorinen. Holographic Dilepton Production in a Thermalizing Plasma. *JHEP*, 1207:094, 2012.
- [6] Vijay Balasubramanian and Simon F. Ross. Holographic particle detection. *Phys.Rev.*, D61:044007, 2000.
- [7] Sayantani Bhattacharyya and Shiraz Minwalla. Weak Field Black Hole Formation in Asymptotically AdS Spacetimes. *JHEP*, 0909:034, 2009.
- [8] J.J Bisognano and E.H. Wichmann. On the Duality Condition for a Hermitian Scalar Field. *J.Math.Phys.*, 16:985–1007, 1975.
- [9] J.J Bisognano and E.H. Wichmann. On the Duality Condition for Quantum Fields. *J.Math.Phys.*, 17:303–321, 1976.
- [10] David D. Blanco, Horacio Casini, Ling-Yan Hung, and Robert C. Myers. Relative Entropy and Holography. *JHEP*, 1308:060, 2013.
- [11] Raphael Bousso, Horacio Casini, Zachary Fisher, and Juan Maldacena. Entropy on a null surface for interacting quantum field theories and the Bousso bound. 2014.
- [12] Raphael Bousso, Ben Freivogel, Stefan Leichenauer, Vladimir Rosenhaus, and Claire Zukowski. Null Geodesics, Local CFT Operators and AdS/CFT for Subregions. *Phys.Rev.*, D88:064057, 2013.

- [13] Raphael Bousso, Stefan Leichenauer, and Vladimir Rosenhaus. Light-sheets and AdS/CFT. *Phys.Rev.*, D86:046009, 2012.
- [14] Pasquale Calabrese and John L. Cardy. Evolution of entanglement entropy in one-dimensional systems. *J.Stat.Mech.*, 0504:P04010, 2005.
- [15] Robert Callan, Jian-Yang He, and Matthew Headrick. Strong subadditivity and the covariant holographic entanglement entropy formula. *JHEP*, 1206:081, 2012.
- [16] H. Casini. Relative entropy and the Bekenstein bound. *Class.Quant.Grav.*, 25:205021, 2008.
- [17] Horacio Casini, Marina Huerta, and Robert C. Myers. Towards a derivation of holographic entanglement entropy. *JHEP*, 1105:036, 2011.
- [18] Bartłomiej Czech, Joanna L. Karczmarek, Fernando Nogueira, and Mark Van Raamsdonk. The Gravity Dual of a Density Matrix. *Class.Quant.Grav.*, 29:155009, 2012.
- [19] Richard A. Davison and Andrei Parnachev. Hydrodynamics of cold holographic matter. *JHEP*, 1306:100, 2013.
- [20] Netta Engelhardt and Aron C. Wall. Quantum Extremal Surfaces: Holographic Entanglement Entropy beyond the Classical Regime. 2014.
- [21] G. Evenbly and G. Vidal. Tensor Network States and Geometry. *Journal of Statistical Physics*, 145:891–918, November 2011.
- [22] Thomas Faulkner, Monica Guica, Thomas Hartman, Robert C. Myers, and Mark Van Raamsdonk. Gravitation from Entanglement in Holographic CFTs. *JHEP*, 1403:051, 2014.
- [23] Thomas Faulkner, Aitor Lewkowycz, and Juan Maldacena. Quantum corrections to holographic entanglement entropy. *JHEP*, 1311:074, 2013.
- [24] Lukasz Fidkowski, Veronika Hubeny, Matthew Kleban, and Stephen Shenker. The Black hole singularity in AdS / CFT. *JHEP*, 0402:014, 2004.
- [25] Ben Freivogel, Steven B. Giddings, and Matthew Lippert. Toward a theory of precursors. *Phys.Rev.*, D66:106002, 2002.
- [26] David Garfinkle and Leopoldo A. Pando Zayas. Rapid Thermalization in Field Theory from Gravitational Collapse. *Phys.Rev.*, D84:066006, 2011.
- [27] Steven B. Giddings and Matthew Lippert. Precursors, black holes, and a locality bound. *Phys.Rev.*, D65:024006, 2002.
- [28] S.S. Gubser, Igor R. Klebanov, and Alexander M. Polyakov. Gauge theory correlators from noncritical string theory. *Phys.Lett.*, B428:105–114, 1998.

- [29] Rudolf Haag and R Haag. *Local quantum physics: Fields, particles, algebras*, volume 2. Springer Berlin, 1996.
- [30] Jutho Haegeman, Tobias J. Osborne, Henri Verschelde, and Frank Verstraete. Entanglement renormalization for quantum fields in real space. *Phys.Rev.Lett.*, 110(10):100402, 2013.
- [31] Thomas Hartman and Juan Maldacena. Time Evolution of Entanglement Entropy from Black Hole Interiors. *JHEP*, 1305:014, 2013.
- [32] Matthew Headrick, Veronika E. Hubeny, Albion Lawrence, and Mukund Rangamani. Causality and holographic entanglement entropy. 2014.
- [33] Idse Heemskerk. Construction of Bulk Fields with Gauge Redundancy. *JHEP*, 1209:106, 2012.
- [34] Idse Heemskerk, Donald Marolf, Joseph Polchinski, and James Sully. Bulk and Transhorizon Measurements in AdS/CFT. *JHEP*, 1210:165, 2012.
- [35] Christoph Holzhey, Finn Larsen, and Frank Wilczek. Geometric and renormalized entropy in conformal field theory. *Nucl.Phys.*, B424:443–467, 1994.
- [36] Gary T. Horowitz and Joseph Polchinski. Gauge/gravity duality. 2006.
- [37] Veronika E. Hubeny and Mukund Rangamani. Causal Holographic Information. *JHEP*, 1206:114, 2012.
- [38] Veronika E. Hubeny, Mukund Rangamani, and Tadashi Takayanagi. A Covariant holographic entanglement entropy proposal. *JHEP*, 0707:062, 2007.
- [39] Ling-Yan Hung, Robert C. Myers, and Michael Smolkin. Twist operators in higher dimensions. *JHEP*, 1410:178, 2014.
- [40] Vivek Iyer and Robert M. Wald. Some properties of Noether charge and a proposal for dynamical black hole entropy. *Phys.Rev.*, D50:846–864, 1994.
- [41] Daniel Kabat, Gilad Lifschytz, and David A. Lowe. Constructing local bulk observables in interacting AdS/CFT. *Phys.Rev.*, D83:106009, 2011.
- [42] Daniel Kabat, Gilad Lifschytz, Shubho Roy, and Debajyoti Sarkar. Holographic representation of bulk fields with spin in AdS/CFT. *Phys.Rev.*, D86:026004, 2012.
- [43] Alexei Kitaev. Talks at KITP, January/April 2015.
- [44] Igor R. Klebanov. String theory in two-dimensions. 1991.
- [45] Aitor Lewkowycz and Juan Maldacena. Generalized gravitational entropy. *JHEP*, 1308:090, 2013.

- [46] Shu Lin and Edward Shuryak. Toward the AdS/CFT Gravity Dual for High Energy Collisions. 3. Gravitationally Collapsing Shell and Quasiequilibrium. *Phys.Rev.*, D78:125018, 2008.
- [47] Shu Lin and Ho-Ung Yee. Out-of-Equilibrium Chiral Magnetic Effect at Strong Coupling. *Phys.Rev.*, D88:025030, 2013.
- [48] Hong Liu and Márk Mezei. Probing renormalization group flows using entanglement entropy.
- [49] Hong Liu and S. Josephine Suh. Entanglement Tsunami: Universal Scaling in Holographic Thermalization.
- [50] Jorma Louko, Donald Marolf, and Simon F. Ross. On geodesic propagators and black hole holography. *Phys.Rev.*, D62:044041, 2000.
- [51] Juan Maldacena and Leonard Susskind. Cool horizons for entangled black holes. *Fortsch.Phys.*, 61:781–811, 2013.
- [52] Juan Martin Maldacena. The Large N limit of superconformal field theories and supergravity. *Int.J.Theor.Phys.*, 38:1113–1133, 1999.
- [53] Donald Marolf, Djordje Minic, and Simon F. Ross. Notes on space-time thermodynamics and the observer dependence of entropy. *Phys.Rev.*, D69:064006, 2004.
- [54] Masamichi Miyaji, Shinsei Ryu, Tadashi Takayanagi, and Xueda Wen. Boundary States as Holographic Duals of Trivial Spacetimes. 2014.
- [55] Masamichi Miyaji and Tadashi Takayanagi. Surface/State Correspondence as a Generalized Holography. 2015.
- [56] Robert C. Myers and Aninda Sinha. Seeing a c-theorem with holography. *Phys.Rev.*, D82:046006, 2010.
- [57] Masahiro Nozaki, Shinsei Ryu, and Tadashi Takayanagi. Holographic Geometry of Entanglement Renormalization in Quantum Field Theories. *JHEP*, 1210:193, 2012.
- [58] Don N. Page. Average entropy of a subsystem. *Phys.Rev.Lett.*, 71:1291–1294, 1993.
- [59] Kyriakos Papadodimas and Suvrat Raju. Black Hole Interior in the Holographic Correspondence and the Information Paradox. *Phys.Rev.Lett.*, 112(5):051301, 2014.
- [60] Kyriakos Papadodimas and Suvrat Raju. State-Dependent Bulk-Boundary Maps and Black Hole Complementarity. *Phys.Rev.*, D89:086010, 2014.

- [61] Joseph Polchinski, Leonard Susskind, and Nicolaos Toumbas. Negative energy, superluminality and holography. *Phys.Rev.*, D60:084006, 1999.
- [62] Shinsei Ryu and Tadashi Takayanagi. Aspects of Holographic Entanglement Entropy. *JHEP*, 0608:045, 2006.
- [63] Shinsei Ryu and Tadashi Takayanagi. Holographic derivation of entanglement entropy from AdS/CFT. *Phys.Rev.Lett.*, 96:181602, 2006.
- [64] Michael Smolkin and Sergey N. Solodukhin. Correlation functions on conical defects. 2014.
- [65] Leonard Susskind and Nicolaos Toumbas. Wilson loops as precursors. *Phys.Rev.*, D61:044001, 2000.
- [66] B. Swingle. Entanglement renormalization and holography. *Physical Review D*, 86(6):065007, September 2012.
- [67] Brian Swingle. Constructing holographic spacetimes using entanglement renormalization. 2012.
- [68] Tadashi Takayanagi and Tomonori Ugajin. Measuring Black Hole Formations by Entanglement Entropy via Coarse-Graining. *JHEP*, 1011:054, 2010.
- [69] Mark Van Raamsdonk. Building up spacetime with quantum entanglement. *Gen.Rel.Grav.*, 42:2323–2329, 2010.
- [70] G. Vidal. Class of Quantum Many-Body States That Can Be Efficiently Simulated. *Physical Review Letters*, 101(11):110501, September 2008.
- [71] Aron C. Wall. Maximin Surfaces, and the Strong Subadditivity of the Covariant Holographic Entanglement Entropy. *Class.Quant.Grav.*, 31(22):225007, 2014.
- [72] Edward Witten. Anti-de Sitter space and holography. *Adv.Theor.Math.Phys.*, 2:253–291, 1998.
- [73] Bin Wu. On holographic thermalization and gravitational collapse of massless scalar fields. *JHEP*, 1210:133, 2012.
- [74] Bin Wu. On holographic thermalization and gravitational collapse of tachyonic scalar fields. *JHEP*, 1304:044, 2013.